PHILOSOPHICAL TRANSACTIONS A

rsta.royalsocietypublishing.org

Research

Article submitted to journal

Subject Areas:
applied mathematics, fluid dynamics, vortex dynamics

Keywords:
Vortex dynamics, surfaces, point vortices

Author for correspondence:
David G. Dritschel
e-mail:
david.dritschel@st-andrews.ac.uk

THE ROYAL SOCIETY PUBLISHING

Equilibria and stability of four point vortices on a sphere

David G. Dritschel

Mathematical Institute, University of St Andrews, St Andrews KY16 9SS, UK

This paper discusses the problem of finding the equilibrium positions of four point vortices, of generally unequal circulations, on the surface of a sphere. A random search method is developed which utilises a modification of the linearised equations to converge on distinct equilibria. Many equilibria (47 and possibly more) may exist for prescribed circulations and angular impulse. A linear stability analysis indicates that they are generally unstable, though stable equilibria do exist. Overall, there is a surprising diversity of equilibria, including those which rotate about an axis opposite to the angular impulse vector.

1. Introduction

The general motion of point vortices on the surface of a sphere is a fascinating and difficult mathematical problem. The nonlinearity of the governing equations greatly impedes analytical progress in all but the simplest situations, either low numbers of vortices ($n < 3$) or highly-symmetric vortex configurations (a comprehensive review can be found in [11]). The lowest number of vortices which can potentially exhibit chaotic motion is $n = 4$, the focus of the present study. It is motivated by a recent study of the late-time behaviour of nearly-inviscid two-dimensional turbulence on the surface of a sphere [7]. There, it was found that the flow organises into four dominant vortices, and these vortices move in an unsteady manner, perhaps indefinitely. It was shown that four point vortices, chosen to have approximately the same circulations as the distributed vortices in the simulation, exhibit the same unsteadiness with the same dominant frequency.

It is plausible that this unsteadiness is generic, i.e. that steady configurations (including uniformly rotating ones) are exceptional. To gain further insight, the objective here is to determine what point vortex equilibria exist and to examine their stability.

Notably, the 4 vortex problem is integrable when the angular impulse vector is identically zero [15], a special case in the present study. The angular impulse vector is the sum of the circulation-weighted Cartesian vector positions. When this is zero (all three components), chaos cannot occur and periodic motion is generic [16]; however, non-self-similar partial collapse (i.e. of 3 of the 4 vortices) may occur when certain conditions are satisfied by the vortex circulations. Collapse cannot occur when the angular impulse vector differs from zero.

The problem of determining point vortex equilibria even for $n = 4$ vortices is challenging because it depends on three independent circulation ratios and the magnitude of the angular impulse, and many solutions exist. A closely-related study [12] developed a novel approach to constructing general point vortex equilibria, for $n = 4$ vortices and greater. In this approach, a "Brownian ratchet" scheme was implemented to solve the linear system for the point vortex circulations, given the inter-vortical distances. To reach a (relative) equilibrium, the vortices are made to carry out a random walk until some 'optimal' basis is obtained for determining the circulations. This permits one to study the 'entropy' and other important properties of general vortex configurations of this type. A generalisation of this approach in [13] starts from 'optimally packed' states, e.g. a tetrahedron for $n = 4$ identical vortices, and finds new equilibria having unequal circulations by the Brownian ratchet scheme above. Equilibria of up to $n = 24$ vortices have been found in this way.

An alternative approach, described here, instead fixes the vortex circulations and the angular impulse vector (without loss of generality along the z axis), then searches for the vortex positions which are in relative equilibrium. This is done by randomly throwing the vortices on the sphere (though one can always be placed at 0 longitude), adjusting them so that they have the correct angular impulse, then relaxing them to a nearby equilibrium using a modification of the linearised dynamics. At each stage of the iteration the vortices must be re-adjusted to have the correct angular impulse. Often, this does not converge. When it does, we obtain an equilibrium. However, the equilibrium may be identical to one already obtained, so it is discarded and further random throws are made in an attempt to find all possible equilibria. There is no guarantee that all can be found, but the results presented below likely cover all possible equilibria except in a few cases, as noted.

On the plane, [1] developed an analogous approach wherein new configurations of equal-circulation vortices are 'grown' from known configurations. First, zero-circulation points are placed at one or more co-rotating points of the configuration, then their circulations are slowly increased while solving a Newton relaxation problem to determine the new vortex positions. In this way, they discovered entirely asymmetric configurations of 8 or more vortices. See also [5] for vortex equilibria existing within a circular disk.

This paper is organised as follows. In the next section, we describe a general approach for calculating the linear stability of any point vortex (relative) equilibrium. This is adapted in section 3 to compute vortex equilibria by a relaxation method. In section 4, equilibria for a variety of circulation ratios are presented along with key properties such as growth rate and rotation rate. This reveals a staggering diversity of solutions. The long-time evolution of some of the unstable equilibria is examined in section 5, and some ideas for future work are given in section 6.

2. Linear stability of general relative equilibria

Below, we describe a general procedure to determine the stability of any uniformly-rotating (relative) equilibrium configuration of point vortices on the unit sphere.

Given an equilibrium configuration $\bar{\boldsymbol{x}}_j$, $j = 1, 2, \ldots, n$, rotating uniformly at rate $\boldsymbol{\Omega}$, it must satisfy

$$\frac{\mathrm{d}\bar{\boldsymbol{x}}_j}{\mathrm{d}t} = \boldsymbol{\Omega} \times \bar{\boldsymbol{x}}_j \tag{2.1}$$

(see next section for a general method to construct equilibria). The general evolution of n point vortices is governed by

$$\frac{\mathrm{d}\boldsymbol{x}_j}{\mathrm{d}t} = \boldsymbol{u}_j = \sum_{i\neq j} \kappa_i \frac{\boldsymbol{x}_i \times \boldsymbol{x}_j}{1 - \boldsymbol{x}_i \cdot \boldsymbol{x}_j} \tag{2.2}$$

where it is understood that the index j ranges over $[1, n]$ henceforth. Here $\kappa_i = \Gamma_i/(4\pi)$ is the 'strength' of vortex i, and Γ_i is its circulation.

Consider, then, the evolution of a small perturbation $\boldsymbol{x}'_j = \boldsymbol{x}_j - \bar{\boldsymbol{x}}_j$ in a frame of reference rotating at rate $\boldsymbol{\Omega}$. Then $\boldsymbol{x}'_j$ satisfies (after linearisation and using (2.1) and (2.2))

$$\frac{\mathrm{d}\boldsymbol{x}'_j}{\mathrm{d}t} = \sum_{i\neq j} \kappa_i \left[\frac{\boldsymbol{x}'_i \times \bar{\boldsymbol{x}}_j + \bar{\boldsymbol{x}}_i \times \boldsymbol{x}'_j}{1 - \bar{\boldsymbol{x}}_i \cdot \bar{\boldsymbol{x}}_j} + \frac{\bar{\boldsymbol{x}}_i \times \bar{\boldsymbol{x}}_j (\boldsymbol{x}'_i \cdot \bar{\boldsymbol{x}}_j + \bar{\boldsymbol{x}}_i \cdot \boldsymbol{x}'_j)}{(1 - \bar{\boldsymbol{x}}_i \cdot \bar{\boldsymbol{x}}_j)^2} \right] - \boldsymbol{\Omega} \times \boldsymbol{x}'_j \,. \tag{2.3}$$

While it is not evident, the perturbation velocity is tangent to the surface of the sphere. It is convenient to make use of this directly by expressing

$$\boldsymbol{x}'_j(t) = a_j(t)\hat{\boldsymbol{e}}_{\mathsf{a}j} + b_j(t)\hat{\boldsymbol{e}}_{\mathsf{b}j} \tag{2.4}$$

where $a_j \ll 1$ and $b_j \ll 1$, while $\hat{\boldsymbol{e}}_{\mathsf{a}j}$ and $\hat{\boldsymbol{e}}_{\mathsf{b}j}$ are unit vectors perpendicular to $\bar{\boldsymbol{x}}_j$. They are constructed as follows. Suppose $|\bar{x}_j| < |\bar{y}_j|$ and $|\bar{x}_j| \leq |\bar{z}_j|$. Then we choose

$$\hat{\boldsymbol{e}}_{\mathsf{a}j} = (h_j, -\bar{x}_j\bar{y}_j/h_j, -\bar{x}_j\bar{z}_j/h_j) \tag{2.5}$$

where $h_j \equiv \sqrt{1 - \bar{x}_j^2}$, so that $\hat{\boldsymbol{e}}_{\mathsf{a}j}$ points predominantly along the positive x axis. Then, we define

$$\hat{\boldsymbol{e}}_{\mathsf{b}j} = \bar{\boldsymbol{x}}_j \times \hat{\boldsymbol{e}}_{\mathsf{a}j}/|\bar{\boldsymbol{x}}_j \times \hat{\boldsymbol{e}}_{\mathsf{a}j}| = (0, \bar{z}_j/h_j, -\bar{y}_j/h_j) \tag{2.6}$$

in this case, so that $\{\hat{\boldsymbol{e}}_{\mathsf{a}j}, \hat{\boldsymbol{e}}_{\mathsf{b}j}, \bar{\boldsymbol{x}}_j\}$ form a right-handed set of unit vectors. The other two cases, i.e. when $|\bar{y}_j| < |\bar{z}_j|$ and $|\bar{y}_j| \leq |\bar{x}_j|$, or when $|\bar{z}_j| < |\bar{x}_j|$ and $|\bar{z}_j| \leq |\bar{y}_j|$, are constructed similarly.

The evolution equations satisfied by a_j and b_j are found by dotting (2.3) into $\hat{\boldsymbol{e}}_{\mathsf{a}j}$ and $\hat{\boldsymbol{e}}_{\mathsf{b}j}$ respectively. The complicated expressions simplify greatly by making use of the general result

$$\boldsymbol{u} \cdot (\boldsymbol{v} \times \boldsymbol{w}) = \boldsymbol{v} \cdot (\boldsymbol{w} \times \boldsymbol{u}) = \boldsymbol{w} \cdot (\boldsymbol{u} \times \boldsymbol{v})$$

for 3 arbitrary vectors $\boldsymbol{u}$, $\boldsymbol{v}$ and $\boldsymbol{w}$, together with $\hat{\boldsymbol{e}}_{\mathsf{a}j} \times \hat{\boldsymbol{e}}_{\mathsf{b}j} = \bar{\boldsymbol{x}}_j$, $\hat{\boldsymbol{e}}_{\mathsf{b}j} \times \bar{\boldsymbol{x}}_j = \hat{\boldsymbol{e}}_{\mathsf{a}j}$ and $\bar{\boldsymbol{x}}_j \times \hat{\boldsymbol{e}}_{\mathsf{a}j} = \hat{\boldsymbol{e}}_{\mathsf{b}j}$. The result is

$$\frac{\mathrm{d}a_j}{\mathrm{d}t} = \sum_{i\neq j} \kappa_i \left[G_{ij}^{ab} a_i + G_{ij}^{bb} b_i - G_{ij}^{xx} b_j + G_{ij}^{xb} \left(G_{ji}^{xa} a_i + G_{ji}^{xb} b_i + G_{ij}^{xa} a_j + G_{ij}^{xb} b_j \right) \right] + b_j \boldsymbol{\Omega} \cdot \bar{\boldsymbol{x}}_j \tag{2.7}$$

$$\frac{\mathrm{d}b_j}{\mathrm{d}t} = -\sum_{i\neq j} \kappa_i \left[G_{ij}^{aa} a_i + G_{ji}^{ab} b_i - G_{ij}^{xx} a_j + G_{ij}^{xa} \left(G_{ji}^{xa} a_i + G_{ji}^{xb} b_i + G_{ij}^{xa} a_j + G_{ij}^{xb} b_j \right) \right] - a_j \boldsymbol{\Omega} \cdot \bar{\boldsymbol{x}}_j \tag{2.8}$$

where

$$\begin{array}{lll} G_{ij}^{xa} = Q_{ij} \bar{\boldsymbol{x}}_i \cdot \hat{\boldsymbol{e}}_{\mathsf{a}j} & G_{ij}^{xb} = Q_{ij} \bar{\boldsymbol{x}}_i \cdot \hat{\boldsymbol{e}}_{\mathsf{b}j} & G_{ij}^{xx} = Q_{ij} \bar{\boldsymbol{x}}_i \cdot \bar{\boldsymbol{x}}_j \\ G_{ij}^{aa} = Q_{ij} \hat{\boldsymbol{e}}_{\mathsf{a}i} \cdot \hat{\boldsymbol{e}}_{\mathsf{a}j} & G_{ij}^{ab} = Q_{ij} \hat{\boldsymbol{e}}_{\mathsf{a}i} \cdot \hat{\boldsymbol{e}}_{\mathsf{b}j} & G_{ij}^{bb} = Q_{ij} \hat{\boldsymbol{e}}_{\mathsf{b}i} \cdot \hat{\boldsymbol{e}}_{\mathsf{b}j} \,, \end{array} \tag{2.9}$$

and $Q_{ij} \equiv (1 - \bar{\boldsymbol{x}}_i \cdot \bar{\boldsymbol{x}}_j)^{-1}$.

Since all of the coefficients above are time-independent in the frame of reference rotating with the unperturbed configuration, we can seek eigen-solutions of the form $a_j(t) = \tilde{a}_j e^{\sigma t}$ and $b_j(t) =$

$\tilde{b}_j e^{\sigma t}$. This results in the matrix-eigenvalue problem

$$\sigma \boldsymbol{v} = \begin{pmatrix} \mathsf{C} & \mathsf{B} \\ -\mathsf{A} & -\mathsf{D} \end{pmatrix} \boldsymbol{v} \quad \text{with} \quad \boldsymbol{v} \equiv \begin{pmatrix} \tilde{\boldsymbol{a}} \\ \tilde{\boldsymbol{b}} \end{pmatrix} \tag{2.10}$$

and where $\tilde{\boldsymbol{a}} \equiv (\tilde{a}_1, \tilde{a}_2, ..., \tilde{a}_n)^T$ and $\tilde{\boldsymbol{b}} \equiv (\tilde{b}_1, \tilde{b}_2, ..., \tilde{b}_n)^T$. The $n \times n$ matrices A, B, C and D in (2.10) are given by

$$\mathsf{A}_{ji} = \kappa_i (G_{ij}^{aa} + G_{ji}^{xa} G_{ij}^{xa}) \tag{2.11}$$

$$\mathsf{B}_{ji} = \kappa_i (G_{ij}^{bb} + G_{ji}^{xb} G_{ij}^{xb}) \tag{2.12}$$

$$\mathsf{C}_{ji} = \kappa_i (G_{ij}^{ab} + G_{ji}^{xa} G_{ij}^{xb}) \tag{2.13}$$

$$\mathsf{D}_{ji} = \kappa_i (G_{ji}^{ab} + G_{ij}^{xa} G_{ji}^{xb}) \tag{2.14}$$

for $i \neq j$ and, otherwise

$$\mathsf{A}_{jj} = \sum_{i \neq j} \kappa_i \left[(G_{ij}^{xa})^2 - G_{ij}^{xx} \right] + \boldsymbol{\Omega} \cdot \bar{\boldsymbol{x}}_j \tag{2.15}$$

$$\mathsf{B}_{jj} = \sum_{i \neq j} \kappa_i \left[(G_{ij}^{xb})^2 - G_{ij}^{xx} \right] + \boldsymbol{\Omega} \cdot \bar{\boldsymbol{x}}_j \tag{2.16}$$

$$\mathsf{C}_{jj} = \mathsf{D}_{jj} = \sum_{i \neq j} \kappa_i G_{ij}^{xa} G_{ij}^{xb} \tag{2.17}$$

Note that each row of the eigen-matrix in (2.10) has a fixed index j. The upper half of (2.10) corresponds to the negative of (2.8), while the lower half corresponds to (2.7). The skew symmetry arises from incompressibility.

There are $2n$ possible eigenmodes for a system of n vortices. However, because the dynamical system is Hamiltonian, the eigenvalues σ come either in pairs, $\sigma = \pm\lambda$, when λ is pure real or pure imaginary, or in quartets, $\sigma = \pm\lambda$ and $\sigma = \pm\lambda^*$ (where $*$ denotes complex conjugate), when λ has non-zero real and imaginary parts.

Moreover, conservation of energy implies that the determinant of the matrix in (2.10) vanishes (thus $\sigma = 0$ is one eigenvalue). Additionally, the form of the eigenvalues noted above implies that the characteristic equation for σ contains only even powers, i.e. it has the general form

$$\sigma^{2n} + c_1 \sigma^{2n-2} + c_2 \sigma^{2n-4} + c_{n-1} \sigma^2 = 0$$

for real coefficients c_1, c_2, ..., c_{n-1}. The non-zero roots therefore are found from a polynomial of degree $n-1$ in σ^2. This polynomial can be further reduced by using conservation of angular impulse, which implies that $\sigma = \pm i\Omega$ must be roots of the above equation. The remaining roots are then found from a polynomial of degree $n-2$ in σ^2. Hence, there can be at most $n-2$ unstable modes for n vortices (this situation has been observed for a particular configuration of 4 vortices with unequal vortex strengths).

We illustrate next the stability of $n = 4$ vortices, on two latitudinal rings located at $\pm\theta$. Two vortices with strengths $\kappa_j = 1$ are placed in the $y = 0$ plane at latitude θ, while the other two vortices with strengths $\kappa_j = -1$ are placed in the $x = 0$ plane at latitude $-\theta$. These rotate about the z axis at the rate $\Omega = 2\sin\theta/\cos^2\theta$. The linear stability analysis above indicates that this configuration is unstable for $\theta > \sin^{-1}(\sqrt{2} - 1) \approx 24.47^\circ$, as shown in figure 1(a). This figure shows the growth rate σ_r versus latitude θ (the growth rate $\sigma_r \to \sqrt{2}$ as $\theta \to 90^\circ$).

The boundary of instability near $\theta = 24.47^\circ$ has been confirmed by direct simulation of the nonlinear equations. An example is provided in figure 1(b), showing the evolution of a slightly perturbed unstable configuration for $\theta = 25^\circ$ (the first vortex is perturbed by increasing y from 0 to 10^{-4} and adjusting x so that $x^2 + y^2 + z^2 = 1$). The instability causes the vortices to move close to another staggered configuration, where they remain for a while before moving close to yet another such configuration, and so on. The successive staggered configurations occur at

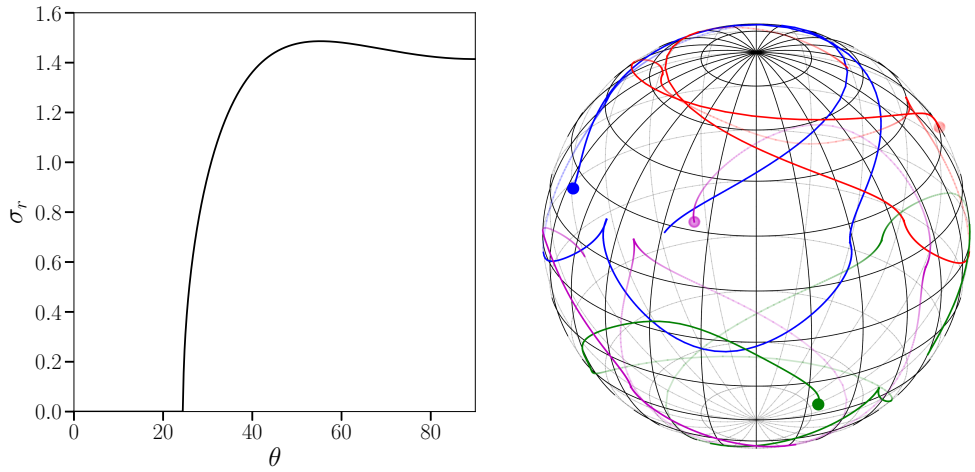

Figure 1. Left: growth rate σ_r versus latitude θ (in degrees) for 4 vortices placed in a staggered configuration, as discussed in the text. Right: trajectories (over $20 \leq t \leq 200$) of 4 unstable vortices perturbed from their initial positions on the latitude circles $\theta = \pm 25°$. The view is orthographic from a latitude of $30°$ and a longitude of $30°$. Lines of constant latitude and longitude are separated by $15°$. Vortices on the far side of the sphere are faded in colour. The final positions of the two positive vortices are shown in blue and red, while those of the two negative vortices are shown in green and magenta.

successive inflections and kinks in the trajectories. The positive vortices remain at nearly the same z positions for all time, as do the negative vortices.

3. Point vortex equilibria: the method

A number of point vortex equilibria (steadily rotating about a fixed axis) are known to exist — one such configuration was illustrated in the previous section. Another is a latitudinal ring of equally-spaced, equal-strength vortices (possibly with additional polar vortices). But these equilibria possess a high degree of symmetry. Here we examine how to construct equilibria having generally different strengths, equilibria that may possess no symmetry at all.

The method developed starts with a guess and tries to iterate a modification of the linearised equations in the previous section to converge to an equilibrium. The full linearised equations cannot be used because the stability matrix is singular (due to conservation of energy). Moreover, there is additional linear dependence expressed through conservation of angular impulse

$$\boldsymbol{I} = \sum_{i=1}^{n} \kappa_i \boldsymbol{x}_i \,. \tag{3.1}$$

This implies

$$\sum_{i=1}^{n} \kappa_i \frac{\mathrm{d}\boldsymbol{x}_i}{\mathrm{d}t} = 0$$

and therefore two of the rows of the stability matrix in (2.10) must be replaced. A third must be replaced because of energy conservation. They are replaced by the linearisation of (3.1), as described next.

Without loss of generality, we can limit our attention to equilibria which steadily rotate about the z axis: $\boldsymbol{\Omega} = \Omega \hat{\boldsymbol{e}}_z$. Such equilibria necessarily have $\boldsymbol{I} = I \hat{\boldsymbol{e}}_z$, i.e. no x and y components of angular impulse. Moreover, we are free to fix the first vortex at zero longitude, $y_1 = 0$ and $x_1 \geq 0$ (the latitude may freely vary). This implies that $\hat{\boldsymbol{e}}_{\mathrm{a}1} = \hat{\boldsymbol{e}}_y$ and hence, from (2.4), that the

perturbation $a_1 = 0$ to keep $y_1 = 0$. This reduces the number of variables to $2n-1$, but another must be added since we must find Ω as part of the solution. The strategy is to take $\Omega = \bar{\Omega} + \Omega'$ where $\bar{\Omega}$ is a guess for the rotation rate, and use Ω' in place of a_1 in the linearised equations to be solved.

The objective, then, is to solve the following set of linearised equations for Ω', a_2, a_3, ..., a_n, and b_1, b_2, ..., b_n starting from a guess $\bar{\boldsymbol{x}}_i$ and $\bar{\Omega}$:

$$\sum_{i\neq j}\kappa_i\left[\frac{\boldsymbol{x}_i'\times\bar{\boldsymbol{x}}_j+\bar{\boldsymbol{x}}_i\times\boldsymbol{x}_j'}{1-\bar{\boldsymbol{x}}_i\cdot\bar{\boldsymbol{x}}_j}+\frac{\bar{\boldsymbol{x}}_i\times\bar{\boldsymbol{x}}_j(\boldsymbol{x}_i'\cdot\bar{\boldsymbol{x}}_j+\bar{\boldsymbol{x}}_i\cdot\boldsymbol{x}_j')}{(1-\bar{\boldsymbol{x}}_i\cdot\bar{\boldsymbol{x}}_j)^2}\right]-\bar{\Omega}\hat{\boldsymbol{e}}_z\times\boldsymbol{x}_j'-\Omega'\hat{\boldsymbol{e}}_z\times\bar{\boldsymbol{x}}_j$$
$$=-\sum_{i\neq j}\kappa_i\frac{\bar{\boldsymbol{x}}_i\times\bar{\boldsymbol{x}}_j}{1-\bar{\boldsymbol{x}}_i\cdot\bar{\boldsymbol{x}}_j}+\bar{\Omega}\hat{\boldsymbol{e}}_z\times\bar{\boldsymbol{x}}_j \quad (3.2)$$

together with

$$\sum_{i=1}^{n}\kappa_i\boldsymbol{x}_i'=I\hat{\boldsymbol{e}}_z-\sum_{i=1}^{n}\kappa_i\bar{\boldsymbol{x}}_i\,, \quad (3.3)$$

where $\boldsymbol{x}_i'$ is defined in (2.4). As done in the linear stability analysis, equations for a_j and b_j (and now Ω') are found by dotting $\hat{\boldsymbol{e}}_{\mathsf{a}j}$ and $\hat{\boldsymbol{e}}_{\mathsf{b}j}$ into (3.2). But to incorporate (3.3), we replace the equation obtained using $\hat{\boldsymbol{e}}_{\mathsf{b}1}$ with the z component of (3.3), and replace the equations obtained using $\hat{\boldsymbol{e}}_{\mathsf{a}n}$ and $\hat{\boldsymbol{e}}_{\mathsf{b}n}$ by the x and y components of (3.3), respectively.

The resulting system of equations reads

$$\begin{pmatrix}\bar{\mathsf{A}} & \bar{\mathsf{D}}\\ \bar{\mathsf{C}} & \bar{\mathsf{B}}\end{pmatrix}\boldsymbol{v}'=\bar{\boldsymbol{R}} \quad (3.4)$$

where $\boldsymbol{v}'\equiv(\Omega', a_2, a_3, ..., a_n, b_1, b_2, ..., b_n)^T$. Here, the upper half of the system is formed by dotting (3.2) into $-\hat{\boldsymbol{e}}_{\mathsf{b}j}$ for rows $j=2$, ..., $n-1$, using the z component of (3.3) for the first row, and using the y component of (3.3) for the nth row. The lower half of the system is formed by dotting (3.2) into $\hat{\boldsymbol{e}}_{\mathsf{a}j}$ for $j=1$, ..., $n-1$, using the x component of (3.3) for $j=n$.

The matrix $\bar{\mathsf{A}}$ is the same as A in the linear stability matrix, except the top row for $i=2$, ..., n reads $\bar{\mathsf{A}}_{1i}=\kappa_i\hat{e}_{\mathsf{a}zi}$ (where $\hat{e}_{\mathsf{a}zi}$ is the z component of $\hat{\boldsymbol{e}}_{\mathsf{a}i}$), the bottom row for $i=2$, ..., n reads $\bar{\mathsf{A}}_{ni}=\kappa_i\hat{e}_{\mathsf{a}yi}$, and the left column for $j=2$, ..., $n-1$ reads $\bar{\mathsf{A}}_{1j}=-\hat{e}_{\mathsf{a}zj}$. Additionally, $\bar{\mathsf{A}}_{11}=\bar{\mathsf{A}}_{n1}=0$. The matrix $\bar{\mathsf{D}}$ is the same as D, except the top row for $i=1$, ..., n reads $\bar{\mathsf{D}}_{1i}=\kappa_i\hat{e}_{\mathsf{b}zi}$, and the bottom row for $i=1$, ..., n reads $\bar{\mathsf{D}}_{ni}=\kappa_i\hat{e}_{\mathsf{b}yi}$. The matrix $\bar{\mathsf{C}}$ is the same as C, except the bottom row for $i=2$, ..., n reads $\bar{\mathsf{C}}_{ni}=\kappa_i\hat{e}_{\mathsf{a}xi}$, and the left column for $j=1$, ..., $n-1$ reads $\bar{\mathsf{C}}_{1j}=-\hat{e}_{\mathsf{b}zj}$. Additionally, $\bar{\mathsf{C}}_{n1}=0$. Finally, the matrix $\bar{\mathsf{B}}$ is the same as B, except the bottom row for $i=1$, ..., n reads $\bar{\mathsf{B}}_{ni}=\kappa_i\hat{e}_{\mathsf{b}xi}$.

The vector $\bar{\boldsymbol{R}}$ appearing on the right-hand side of (3.4) has the following entries. Associated with angular impulse conservation, we have

$$\bar{R}_1=I-\sum_{i=1}^{n}\kappa_i\bar{z}_i\,,\qquad \bar{R}_n=-\sum_{i=1}^{n}\kappa_i\bar{y}_i \quad\text{and}\quad \bar{R}_{2n}=-\sum_{i=1}^{n}\kappa_i\bar{x}_i\,. \quad (3.5)$$

The remaining entries are

$$\bar{R}_j=\bar{\Omega}\hat{e}_{\mathsf{a}zj}-\sum_{i\neq j}\kappa_i G_{ij}^{xa}\quad (j=2,\ ...,\ n-1)\quad\text{and} \quad (3.6)$$

$$\bar{R}_{n+j}=\bar{\Omega}\hat{e}_{\mathsf{b}zj}-\sum_{i\neq j}\kappa_i G_{ij}^{xb}\quad (j=1,\ ...,\ n-1)\,, \quad (3.7)$$

where G_{ij}^{xa} and G_{ij}^{xb} are defined in (2.9).

These linearised equations at best provide a better approximation to an equilibrium (assuming convergence), so in practice they must be iterated until either the r.m.s. value of the corrections $\boldsymbol{x}_i'$ is smaller than a prescribed tolerance (here 10^{-12}), or the corrections diverge. When convergence occurs, the method approaches the equilibrium exponentially fast, with errors falling by more

than a factor of two each step. Often however the equilibrium found is identical to one previously found and must therefore be rejected.

Starting from a known equilibrium say for equal $|\kappa_i|$, it is easy to construct nearby equilibria with slightly unequal strengths, and this can be continued in small steps to construct equilibria with greatly varying $|\kappa_i|$. Alternatively, one can specify arbitrary vortex strengths, then search for equilibria by first choosing the vortex positions at random, adjusting them to have the prescribed value of angular impulse, then iterating from this guess. Generally, this leads to divergence, but some random initial guesses do converge to equilibria. This approach enables one to find multiple equilibria occurring for the same angular impulse. The associated numerical algorithm is described in the following section.

4. Examples of families of non-symmetric point vortex equilibria

We next present several examples of non-symmetric equilibria for $n = 4$ vortices. The equilibria depend on three strength ratios, $\kappa_2/|\kappa_1|$, $\kappa_3/|\kappa_2|$ and $\kappa_4/|\kappa_3|$ as well as the value of the (z-component of) angular impulse I. Without loss of generality, we may take $\kappa_1 > 0$ and largest in magnitude, and the three strength ratios to lie in the range $[-1, 1]$. Moreover, we may require $\sum_i |\kappa_i| = n = 4$, as this effectively sets the time scale (the unit radius of the sphere sets the length scale). We can also restrict attention to $I \geq 0$ since equilibria for $I < 0$ may be obtained simply by flipping the sign of all $\bar{z}_i$ (these also rotate in the opposite direction). Then, since $|\bar{z}_i| \leq 1$ for all vortices, it follows that $I \leq n$, with equality only when all vortices are at the poles: $\bar{z}_i = \kappa_i/|\kappa_i|$.

(a) The search algorithm

The algorithm developed for any $n > 2$ is described next. Starting at $I = 0.9n$ as explained below, the $\bar{z}_i$ for $i > 1$ are chosen randomly from a uniform distribution over $[-1, 1]$, then the definition of I is used to obtain $\bar{z}_1$ from $(I - \sum_{i>1} \kappa_i \bar{z}_i)/\kappa_1$. However, if $\bar{z}_1$ so obtained is greater than 1 in magnitude, we choose a different random set of $\bar{z}_i$ for $i > 1$ and repeat this until $|\bar{z}_1| \leq 1$.

Next, the longitudes φ_i of the vortices are chosen. The first φ_1 must be set to 0 to exclude otherwise identical equilibria that are simple rotations about the z axis. The remaining φ_i cannot be chosen entirely at random since we need to ensure that the x and y components of the angular impulse vector $\boldsymbol{I}$ are zero. The following procedure ensures these components are zero.

First, we sort $|k_i|$, where $k_i = \kappa_i \bar{r}_i$ and $\bar{r}_i = \sqrt{1 - \bar{z}_i^2}$, from largest to smallest. We denote $\tilde{k}_1$ as the largest k_i and $\tilde{k}_n$ as the smallest k_i. In general, $\tilde{k}_1 \geq \tilde{k}_2 \geq \ldots \geq \tilde{k}_n$. Let the corresponding (sorted) longitudes be denoted $\tilde{\varphi}_j$, for $j = 1, \ldots, n$. We select $\tilde{\varphi}_j$ for $j > 2$ randomly from a uniform distribution over $[-\pi, \pi]$. The remaining two longitudes, $\tilde{\varphi}_1$ and $\tilde{\varphi}_2$, are found by requiring the x and y components of the angular impulse are zero, equivalent to requiring

$$\sum_{j=1}^{n} \tilde{k}_j \cos\tilde{\varphi}_j = 0 \quad \Rightarrow \quad \tilde{k}_1 \cos\tilde{\varphi}_1 + \tilde{k}_2 \cos\tilde{\varphi}_2 + \sum_{j=3}^{n} \tilde{k}_j \cos\tilde{\varphi}_j = 0 \tag{4.1}$$

$$\sum_{j=1}^{n} \tilde{k}_j \sin\tilde{\varphi}_j = 0 \quad \Rightarrow \quad \tilde{k}_1 \sin\tilde{\varphi}_1 + \tilde{k}_2 \sin\tilde{\varphi}_2 + \sum_{j=3}^{n} \tilde{k}_j \sin\tilde{\varphi}_j = 0\,. \tag{4.2}$$

The goal is to solve these two equations for $\tilde{\varphi}_1$ and $\tilde{\varphi}_2$, then perform a rigid rotation about the z axis so that the longitude φ_1 of vortex 1 is zero. This rotation leaves the x and y components of the angular impulse at zero.

An analytical solution is found by moving $\tilde{k}_2 \cos\tilde{\varphi}_2$ and $\tilde{k}_2 \sin\tilde{\varphi}_2$ to the right hand sides of (4.1) and (4.2) then squaring and adding the two equations to eliminate $\tilde{\varphi}_2$. This results in an equation of the form

$$A\cos\tilde{\varphi}_1 + B\sin\tilde{\varphi}_1 + C = 0$$

for some constants A, B and C (details not provided). One can then move $B\sin\tilde{\varphi}_1$ to the right hand side, square both sides, and replace $\sin^2\tilde{\varphi}_1$ by $1 - \cos^2\tilde{\varphi}_1$ to obtain a quadratic equation for

$\cos\tilde{\varphi}_1$. If there are no real roots, the above procedure is repeated starting from randomly selected values of $\bar{z}_i$ for $i>1$. Otherwise, one of the two roots (both of which are valid) are selected at random. Then, we directly obtain $\sin\tilde{\varphi}_1$ from $-(A\cos\tilde{\varphi}_1+C)/B$, as well as $\cos\tilde{\varphi}_2$ and $\sin\tilde{\varphi}_2$ from (4.1) and (4.2).

Next, the original sorting is used to find the $\cos\varphi_i$ and $\sin\varphi_i$, for all i, from the $\cos\tilde{\varphi}_j$ and $\sin\tilde{\varphi}_j$, $j=1,\ ...,\ n$. This allows us to determine the x and y positions of the vortices from

$$\bar{x}_i=\bar{r}_i\cos\varphi_i\,,\qquad \bar{y}_i=\bar{r}_i\sin\varphi_i\,.$$

Finally, these coordinates are rotated by φ_1 about the z axis so that the first vortex lies at $\bar{x}_1=\bar{r}_1$ and $\bar{y}_1=0$.

At this stage, we have a guess for the positions $\bar{\boldsymbol{x}}_i$ of all of the vortices consistent with the specified angular impulse $\boldsymbol{I}=I\hat{\boldsymbol{e}}_z$. This is generally not in equilibrium. Moreover, we also need a guess for the rotation rate $\bar{\Omega}$ of the configuration about the z axis. Here, we use the average value of $\mathrm{d}\varphi_i/\mathrm{d}t$, i.e.

$$\bar{\Omega}=\frac{1}{n}\sum_{i=1}^{n}\frac{\bar{x}_i\bar{v}_i-\bar{y}_i\bar{u}_i}{\bar{x}_i^2+\bar{y}_i^2} \tag{4.3}$$

where $\bar{u}_i$ and $\bar{v}_i$ are found using (2.2). We then form the linear system (3.4) and solve it for the perturbations a_j and b_j in (2.4) as well as for the correction Ω' to the rotation rate. The corrections to the point vortex positions $\boldsymbol{x}_j'$ are then added to $\bar{\boldsymbol{x}}_j$, which are subsequently normalised to ensure that they have unit length. Likewise Ω' is added to $\bar{\Omega}$. This is now a corrected guess for an equilibrium. We again form and solve the linear system and do this repeatedly until either it diverges (r.m.s. displacement $\boldsymbol{x}_j'$ exceeds 1) or converges. The latter is said to occur when both the r.m.s. displacement $\boldsymbol{x}_j'$ is less than 10^{-12} and the r.m.s. velocity in the rotating frame of reference, $\bar{\boldsymbol{u}}_j-\bar{\Omega}\hat{\boldsymbol{e}}_z\times\bar{\boldsymbol{x}}_j$, is less than 10^{-11}.

Once an equilibrium is found, it is first checked to see if it is distinct. This is done by comparing the rotation rate $\Omega=\bar{\Omega}$ and energy E, defined by

$$E=-\sum_j\sum_{i\neq j}\kappa_i\kappa_j\ln(1-\boldsymbol{x}_i\cdot\boldsymbol{x}_j)\,, \tag{4.4}$$

with those of any equilibria previously found, say $m=1,\ ...,\ M$. Specifically, we require the difference norm

$$\max_m\ \frac{|q-q_m|}{1+\sqrt{|q\,q_m|}}>10^{-8} \tag{4.5}$$

for $q=\Omega$ *or* E. The choice of this norm is motivated by the fact that both Ω and E are sign indefinite and may vary considerably in magnitude.

The algorithm attempts to find 200 equilibria from 40000 initial guesses before moving on to the next value of I, and moreover up to 20000 attempts are allowed to obtain an initial guess. Of these 200 equilibria, many may be duplicates; in practice from 1 to 47 equilibria are found for $n=4$ vortices (there may be cases having more equilibria; 47 is the maximum so far observed). The numbers 200, 40000 and 20000 are limited by computational cost, but they appear large enough to capture most equilibria.

After these equilibria have been found for the starting value of I, here $I=0.9n$, we decrease I by 0.005 and repeat the procedure, except that we use the equilibria found for the previous value of I as starting guesses for the new equilibria. Normally, for a small difference in I, the equilibria are close to each other. Exceptions occur at the critical values of I for which the vortices are located at either pole; these are the positive values of

$$I_c=\sum_i\kappa_i s_i \tag{4.6}$$

where each s_i can be $+1$ or -1. At these points, branches of solutions (varying with I) terminate or originate (see results below).

The starting value $I=0.9n$ is less than the maximum value $I=n$ for which all vortices are at the pole having the sign of its circulation, i.e. $\bar{z}_i=\kappa_i/|\kappa_i|$. The algorithm requires that the vortices

be separated and cannot be used to find such states, though clearly they are trivial: lumping vortices at the two poles is always an equilibrium. The starting value $I = 0.9n$ is sufficiently large to illustrate the diversity of equilibria possible. Higher values of I produce equilibria which are analogous to those for $I = 0.9n$, only the vortices are closer to the poles.

The angular impulse is decreased all the way to $I = 0$ in this way, then it is increased again in increments of 0.005 back to $I = 0.9n$, using equilibria at the previous value of I as first guesses as well as 20000 completely new guesses (as described above). This enables one to capture new equilibria not found when decreasing I. This completes one 'cycle'. Altogether, the algorithm carries out 10 complete cycles before finishing. This means that, for each value of I, 400000 guesses are made to find the equilibria. Even so, there are cases where it appears some equilibria have been missed, perhaps due to their close proximity to others.

(b) Examples

We next present a few examples for $n = 4$ vortices having generally unequal strengths κ_i. A comprehensive exploration of parameter space is out of the question due to the high computational cost involved (typically 1–3 days on an Intel i7-4712HQ processor clocked at 2.3GHz). Here we focus on a few distinct examples to show the extraordinary variation which occurs.

(i) Equal vortices: $\kappa_1 = \kappa_2 = \kappa_3 = \kappa_4 = 1$

We begin with the simplest case of identical vortices: $\kappa_i = 1$, $\forall i$. In this case, it is simple to work out many of the possible equilibrium forms using symmetry; however, there is one configuration which has relatively little symmetry. For reference, the configurations observed fall into one of seven possible forms:

1. **4-0**, a ring configuration in which all vortices have the same z position and are equally spaced in longitude; this is unstable when $|z| < 1/\sqrt{3}$ [14] or here when $I = 4z < 4/\sqrt{3} \approx 2.3094$;
2. **1-3**, a vortex at the north pole with three others in a ring configuration at height z; this has $I = 1 + 3z$ so $z \geq -\frac{1}{3}$ as $I \geq 0$; this configuration is always stable [3] (see also [4]);
3. **3-1**, a vortex at the south pole with three others in a ring configuration at height z; this has $I = 3z - 1$ so $z \geq \frac{1}{3}$ as $I \geq 0$; this branch only exists up to $I = 2$ where there ring coalesces into a single vortex at the north pole; this configuration is always stable [3];
4. **2-2c**, two pairs of vortices having the same z and opposite x lying on the great circle $y = 0$, i.e. at positions $(\pm\sqrt{1 - z_1^2}, 0, z_1)$ and $(\pm\sqrt{1 - z_2^2}, 0, z_2)$ with $z_1 \neq z_2$; these have $I = 2(z_1 + z_2)$ and are always unstable;
5. **2-2s**, two staggered pairs of vortices having the same z and opposite x or y, i.e. at positions $(\pm\sqrt{1 - z_1^2}, 0, z_1)$ and $(0, \pm\sqrt{1 - z_2^2}, z_2)$ with $z_1 \neq z_2$; these have $I = 2(z_1 + z_2)$ and exist only up to $I = 4/\sqrt{3}$ at which point $z_1 = z_2$ and the solution branches merges into the **4-0** branch; this staggered configuration is stable for $I > \sqrt{2}$;
6. **1-2-1**, a vortex at the north and the south poles with two others in a ring configuration at height z, i.e. at $(\pm\sqrt{1 - z^2}, 0, z)$; this is also a great circle configuration; as $I = 2z$ this configuration exists only for $I \leq 2$; it is always unstable [3];
7. **2-1-1**, two vortices with the same z positions and two others with different z positions not at the poles, i.e. $(\sqrt{1 - z_1^2}, 0, z_1)$, (x_2, y_2, z_1), (x_3, y_3, z_3), and (x_4, y_4, z_4); notably $\varphi_2 = \tan^{-1}(y_2/x_2) < \pi$ in general so the first two vortices are not generally opposite one another; the other two vortices have $z_4 > z_3 > z_1$ and lie in a plane bisecting the first two vortices and have $\varphi_4 = \varphi_3 + \pi$; this configuration exists only for $I \geq \sqrt{2}$ where it emerges as a bifurcation from the **2-2s** branch; it is always unstable.

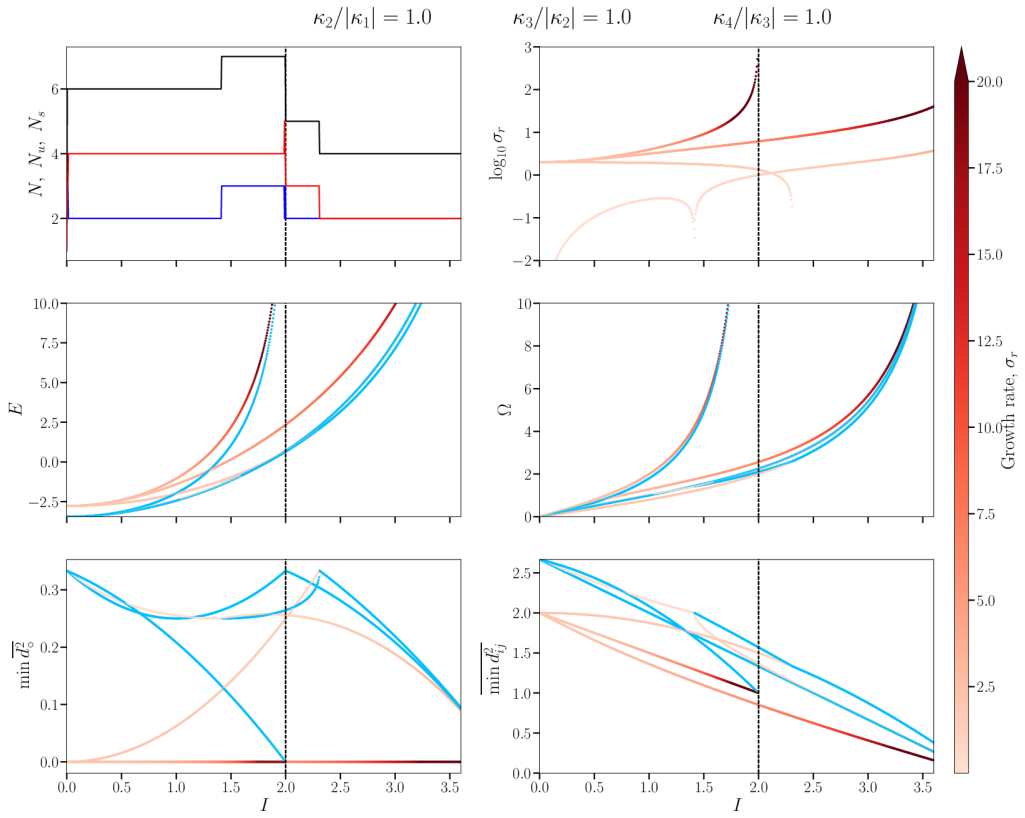

Figure 2. Various properties of point vortex equilibria, as a function of the z component of angular impulse I, for $n = 4$ vortices and when all strengths are equal: $\kappa_i = 1$, $\forall i$. In the upper left panel, the total number N of equilibria is shown in black, the unstable number N_u in red, and the stable number N_s in blue. The remaining panels show the log-scaled growth rate σ_r, the vortex interaction energy E, the equilibrium rotation rate Ω, the minimum average squared distance to a great circle plane $\min \overline{d_\circ^2}$, and the average minimum squared distance between any distinct pair of vortices $\overline{\min d_{ij}^2}$. The latter reaches a maximum of $8/3$ when the vortices are at the vertices of a regular tetrahedron. Blue curves in these panels indicate stable configurations while the red curves indicate unstable ones, with the intensity indicating growth rate (see colour bar at right) capped at 20. The dashed vertical lines indicate the critical values of I in (4.6) where two or more point vortices are at either pole. At these points, E and Ω diverge. There is another critical value at $I = 4$ not shown in this view. At this value, every vortex is at a pole (here the north pole).

Various equilibrium properties of these configuration, as well as linear stability, are shown as a function of I in figure 2. Here, $\min \overline{d_\circ^2}$ is computed by finding the great circle plane $\boldsymbol{m} \cdot \boldsymbol{x} = 0$ for which the average (perpendicular) squared distance to the vortices is minimal. This minimisation determines the vector $\boldsymbol{m}$ (which may be taken to have unit length), from which

$$\min \overline{d_\circ^2} = \frac{1}{n} \sum_{i=1}^{n} |\kappa_i| (\boldsymbol{m} \cdot \boldsymbol{x}_i)^2 \tag{4.7}$$

is calculated (using squared distances weighted by $|\kappa_i|$; recall these weights sum to n). The average minimum squared distance between any distinct pair of vortices is computed from

$$\overline{\min d_{ij}^2} = \frac{1}{n} \sum_{j=1}^{n} \min_{i \neq j} |\boldsymbol{x}_i - \boldsymbol{x}_j|^2. \tag{4.8}$$

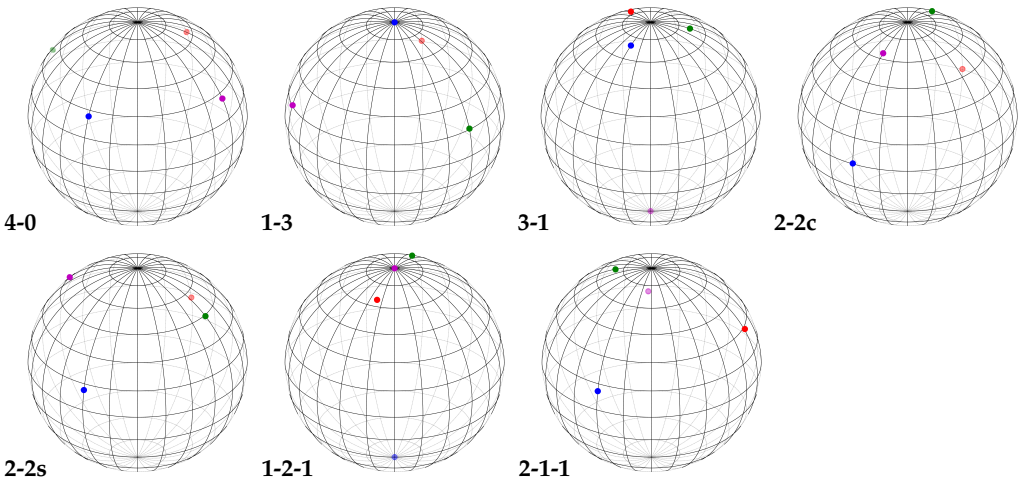

Figure 3. Illustration for equal-strength vortices of the various configurations (as labelled in the lower right) that exist when $I = 1.8$. The view is orthographic from a latitude of 30° and a longitude of 30°. Lines of constant latitude and longitude are separated by 15°. Vortices on the far side of the sphere are faded in colour. Vortex 1 is shown in blue, 2 in red, 3 in green and 4 in magenta.

In the range $\sqrt{2} < I < 2$, every configuration discussed above is present, three of which are stable (**4-0**, **1-3** and **3-1**), and four of which are unstable (**2-2c**, **2-2s**, **1-2-1**, and **2-1-1**). Figure 3 provides a three-dimensional view of these configurations at $I = 1.8$. Starting at $I = 0$, it appears that there are 6 equilibria, but in fact there are just 2. One of them bifurcates from a regular tetrahedron into **1-3**, **3-1** and **2-2s** (all stable) and the other bifurcates from an equally spaced ring into **4-0**, **2-2s** and **1-2-1** (all unstable with a growth rate $\sigma_r = 2$). When $I = 0$, these are just ring configurations on great circles. For small I, it appears that there are 3 stable an 3 unstable equilibria, but in fact only **1-3** and **3-1** are stable. This is because numerical inaccuracies when computing growth rates for configurations with close vortices forced using $\sigma_r < 10^{-4}$ as the criterion for stability. In fact, **2-2s** is weakly unstable with $\sigma_r \approx 0.48713 I^2$ for small I.

Focusing on the stable configurations first, the **3-1** branch (with one vortex at the south pole and the others in a ring) is the short blue curve in each of the 4 bottom panels between $I = 0$ and 2. The long continuous blue curve existing for all I corresponds to the **1-3** branch (with one vortex at the north pole and the others in a ring). The blue curve emerging at $I = \sqrt{2}$ and disappearing at $I = 4/\sqrt{3}$ is the stable portion of the **2-2s** branch of staggered vortices (there is an unstable portion for $0 < I < \sqrt{2}$). It is seen most clearly in the panel for $\min \overline{d_\circ^2}$ as the upward bending loop ending at the peak in this quantity at $I = 4/\sqrt{3}$. A final stable branch, corresponding to the pure ring configuration **4-0**, emerges at $I = 4/\sqrt{3}$ and continues for all larger I; this branch becomes unstable for smaller I.

Turning next to the unstable configurations, it is simplest to refer to the panel showing the log-scaled growth rate. There, the most unstable curve existing only for $I < 2$ corresponds to the **1-2-1** branch having two polar vortices at opposite poles and two other vortices with the same z between 0 (when $I = 0$) and 1 (when $I = 2$). The vortices always lie on a great circle in the $y = 0$ plane ($\min \overline{d_\circ^2} = 0$). The growth rate diverges as $I \to 2$. The next most unstable configuration for $I \le 2$, and most unstable for $I > 2$, is **2-2c**, where the vortices lie on a great circle, two vortices at $z = z_1$ and two others at $z = z_2$. This configuration also has the highest energy E and rotation rate Ω for $I > 2$, and the lowest $\overline{\min d_{ij}^2}$. The third most unstable configuration for $I \le 2$ is the regular ring **4-0**. This is unstable up to $I = 4/\sqrt{3}$ (where $z = 1/\sqrt{3}$ for all vortices) and is stable for all greater I. In $\min \overline{d_\circ^2}$ this configuration is seen as the upward sloping curve until $I = 4/\sqrt{3}$,

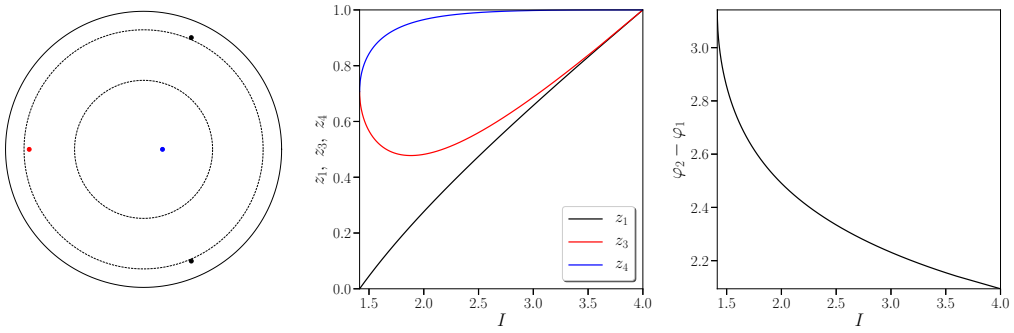

Figure 4. Projected (x, y) positions (left) of the vortices for $I = 2.5$ (when all vortices have equal strength), with the equal height vortices 1 and 2 shown in black, vortex 3 in red, and vortex 4 in blue (the circles show latitudes 0, $\pi/6$ and $\pi/3$); z positions (middle) and angle between the equal height vortices (right) for the **2-1-1** configuration. This exists over the range $\sqrt{2} \leq I \leq 4$. At $I = \sqrt{2}$, the configuration bifurcates from **2-2s** for which $z_3 = z_4 = \sqrt{2}/2$ and $\varphi_2 - \varphi_1 = \pi$. As $I \to 4$, all vortices approach the north pole while $\varphi_2 - \varphi_1 \to 2\pi/3$.

thereafter becoming the upper blue downward sloping curve. In $\overline{\min d_{ij}^2}$, this is the curve starting with zero slope at $I = 0$ and gradually bending downwards, turning stable beyond $I = 4/\sqrt{3}$. The weak instability occurring in the range $0 < I < \sqrt{2}$ corresponds to the staggered **2-2s** branch of solutions; this branch becomes stable for $I > \sqrt{2}$ before terminating at $I = 4/\sqrt{3}$, where it merges into the **4-0** branch. In $\min \overline{d_\circ^2}$, it is the uppermost red curve for small I turning blue at $I = \sqrt{2}$ (where the **2-1-1** configuration emerges) and terminating with a vertical slope at $I = 4/\sqrt{3}$. In $\overline{\min d_{ij}^2}$, it is also the uppermost red curve for $0 < I < \sqrt{2}$ and the uppermost blue curve for $\sqrt{2} < I < 4/\sqrt{3}$. The kink in the curve at $I = \sqrt{2}$ is real. Finally, the instability emerging at $I = \sqrt{2}$, and becoming the second most unstable for $I > 2.115$ approximately, corresponds to the **2-1-1** configuration having only two equal z positions and two other z positions straddling the north pole — the most asymmetric configuration. In $\min \overline{d_\circ^2}$, it is the upper red curve for $I > 4/\sqrt{3}$, while in $\overline{\min d_{ij}^2}$, it is the upper red curve moving down from its value of 2 at $I = \sqrt{2}$ before asymptoting the diagonal blue curve corresponding to the stable **1-3** branch.

Some details of the **2-1-1** configuration across the entire range of its existence are provided in figure 4. In the left panel, the vortex positions are shown projected on the x-y plane for the specific value $I = 2.5$; the middle panel shows the z positions of the vortices (the equal height vortices in black, while the other two in red and blue) as a function of I; the right panel shows the longitudinal separation of the equal height vortices. For this configuration $z_4 > z_3 > z_2 = z_1 > 0$ and vortices 3 and 4 lie in the plane which bisects vortices 1 and 2 ($y = 0$ in the left panel). The vortices do not form a regular tetrahedron.

(ii) One opposite vortex: $\kappa_1 = \kappa_2 = \kappa_3 = 1$ and $\kappa_4 = -1$

Before considering more complex cases, we briefly examine the simplest one found, namely for three equal vortices $\kappa_1 = \kappa_2 = \kappa_3 = 1$ and one opposite vortex $\kappa_4 = -1$. In this case, the fewest equilibria have been found to occur: only up to 5 for any value of the angular impulse I.

The results are summarised in figure 5 in the same format used previously for all equal vortices. At $I = 0$, there are only two configurations, **1˙-3** where the negative vortex is at the north pole and the remaining vortices lie on a regular ring (here at $z = \frac{1}{3}$), and **3-1˙** where the negative vortex is at the south pole and the remaining vortices lie on a regular ring (here at $z = -\frac{1}{3}$). Both are linearly stable [3] at $I = 0$. As $I = 3z - 1$ for **1˙-3**, this configuration exists only for $I < 2$ (since $z < 1$). On the other hand, $I = 3z + 1$ for **3-1˙**, and thus it exists for all I in $[0, 4]$. For small $I > 0$, three additional configurations emerge, two of which are unstable. The stable one **1-1-1˙-1** lies on

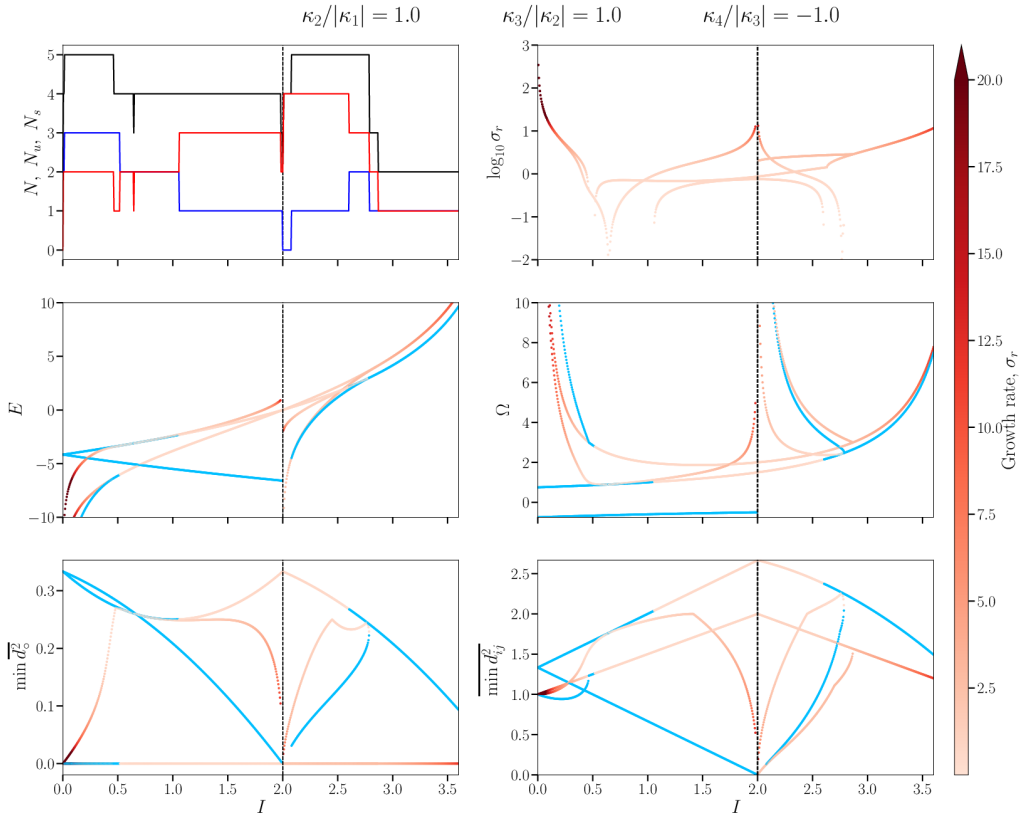

Figure 5. Various properties of point vortex equilibria, as a function of the z component of angular impulse I, for $n = 4$ vortices and for strengths $\kappa_1 = \kappa_2 = \kappa_3 = 1$ and $\kappa_4 = -1$. The layout of the figure is exactly as described in figure 2. The glitch in the number of configurations around $I = 0.65$ in the upper left panel is numerical, and is caused by the existence of two nearly identical states at this value.

a great circle ($y = 0$) but all values of z differ (and the negative vortex does not always occupy the minimum z value). This configuration only exists up to $I = 0.465$ approximately, when it merges into the **1-2-1**$^-$ great circle configuration. The latter has a positive vortex at the north pole, a negative one at the south pole, and the remaining two on a ring of constant z (with $z = I/2 - 1$). This is unstable for small I but becomes stable when it merges with the **1-1-1**$^-$**-1** configuration around $I = 0.465$, then becomes unstable again around $I = 0.519$ and remains unstable for all larger I. The final configuration **2-1**$^-$**-1** has two positive vortices at the same height and in a vertical plane perpendicular to that containing the remaining two vortices (this is similar to the **2-1-1** configuration for all equal vortices discussed above). All the z positions lie between the poles, and again the negative vortex can change order in z with one of the positive vortices. Figure 6 provides a three-dimensional view of these configurations at $I = 2.5$.

The **2-1**$^-$**-1** configuration is unstable up to $I = 2$ where all vortices converge on the north pole and the growth rate diverges. Further properties of this configuration are shown in figure 7, the analogue of figure 4 for all equal vortices. For $I < 2$, there is one **2-1**$^-$**-1** configuration, but for $2 < I < 2.787$ approximately, there are two, one stable and the other unstable. The stable one has the two equal height vortices closer to the north pole (the filled circles in the left panel), a higher rotation rate Ω and a closer average vortex separation (smaller $\overline{\min d_{ij}^2}$). It is also closer to a great circle (smaller $\min \overline{d_\circ^2}$). In $\min \overline{d_\circ^2}$, the two configurations are the middle two curves in figure 5

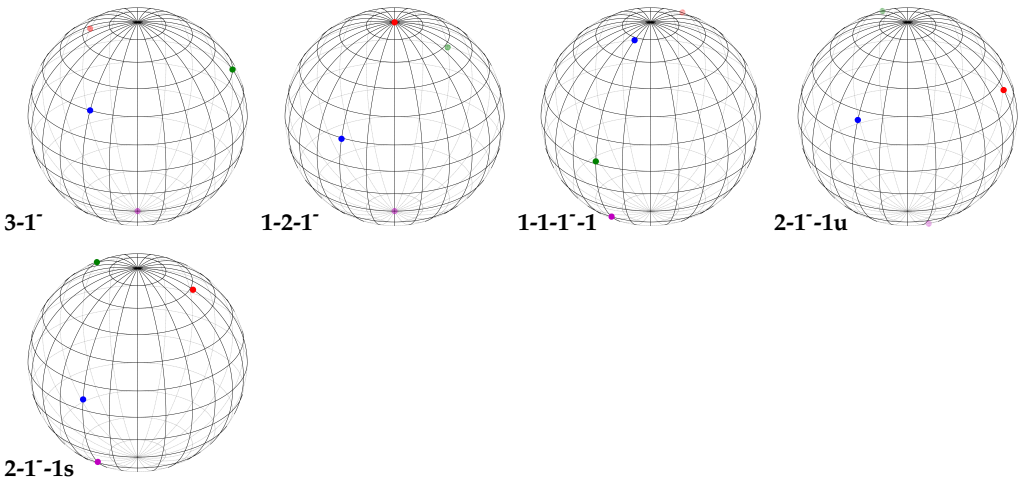

Figure 6. Illustration for $\kappa_1 = \kappa_2 = \kappa_3 = 1$ and $\kappa_4 = -1$ of the various configurations (as labelled in the lower right) that exist when $I = 2.5$. Note there are two **2-1⁻-1** configurations, one unstable labelled 'u' and one stable labelled 's'. The layout is exactly as in figure 3. Vortex 1 is shown in blue, 2 in red, 3 in green and 4 in magenta.

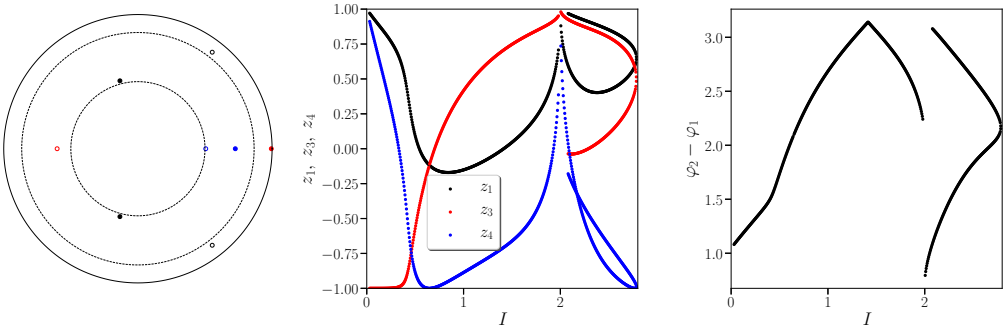

Figure 7. Projected (x, y) positions (left) of the vortices (when $\kappa_1 = \kappa_2 = \kappa_3 = 1$ and $\kappa_4 = -1$) for the **2-1⁻-1** configuration at $I = 2.5$, with the equal height vortices 1 and 2 shown in black, vortex 3 in red, and vortex 4 (negative) in blue; the filled and open circles belong to different configurations of this type (the format is the same as in figure 4); z positions of the vortices (middle) versus I; and angle between the equal height vortices (right). This exists over the range $0 < I < 2.787$ approximately, where the two different configurations coalesce (they do not continue as another configuration for larger I).

(blue and red), while in $\overline{\min d_{ij}^2}$ they are the upper two curves with positive slope (also blue and red). Note, when $I = \sqrt{2}$, vortices 1 and 2 lie on the equator and are opposite one another ($\boldsymbol{x}_1 = (0, -1, 0)$ and $\boldsymbol{x}_2 = (0, 1, 0)$), while vortices 3 and 4 lie above one another at $\pm 45^\circ$ degrees latitude ($\boldsymbol{x}_3 = (1, 0, 1)/\sqrt{2}$ and $\boldsymbol{x}_4 = (1, 0, -1)/\sqrt{2}$).

Returning to figure 5, the stable **1⁻-3** configuration (with the negative vortex at the north pole) exists only up to $I = 2$ when all vortices reach the north pole. This is the only counter-rotating configuration ($\Omega < 0$), and can be seen by the nearly straight blue lines in the lower 4 panels of the figure between $I = 0$ and 2. The **3-1⁻** configuration (with the negative vortex at the south pole) exists for all I but is unstable in the range $1.055 < I < 2.602$ approximately. This is the upper curve

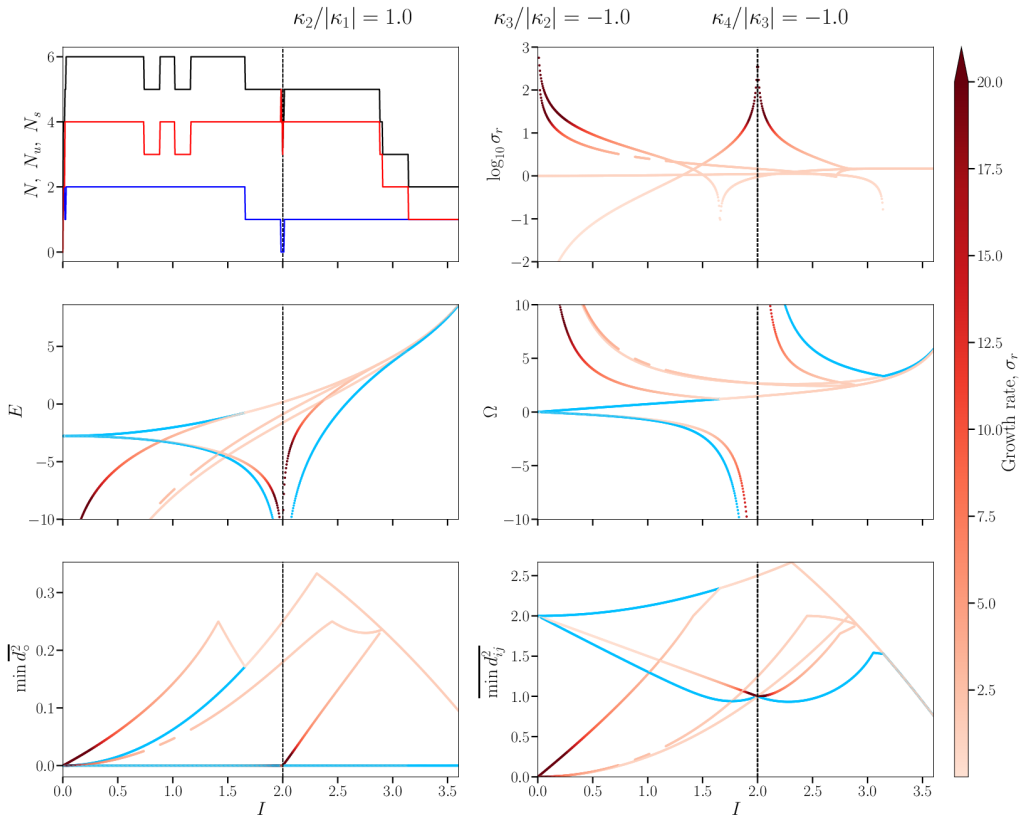

Figure 8. Various properties of point vortex equilibria, as a function of the z component of angular impulse I, for $n = 4$ vortices and for strengths $\kappa_1 = \kappa_2 = 1$ and $\kappa_3 = \kappa_4 = -1$. The layout of the figure is exactly as described in figure 2.

in $\overline{\min d_{ij}^2}$ over the whole range of I and also in $\min \overline{d_\circ^2}$ for most of the range. The **1-2-1**$^-$ great circle configuration with two polar vortices is the tent shaped curve reaching a maximum of 2 at $I = 2$ in $\overline{\min d_{ij}^2}$. It has a small window of stability as already noted around $I = 0.5$. The red curve with the kink in $\overline{\min d_{ij}^2}$ for $I < 2$ is the **2-1**$^-$**-1** configuration already discussed above. For $I > 2$, there is one additional configuration seen as the lowest red curve with positive slope in $\overline{\min d_{ij}^2}$. This is another great circle configuration **1-1-1-1**$^-$, and it terminates near $I = 2.87$ where it merges into the **1-2-1**$^-$ configuration.

(iii) Two opposite vortices: $\kappa_1 = \kappa_2 = 1$ and $\kappa_3 = \kappa_4 = -1$

The last 'simple' case to consider is the anti-symmetric one for equal magnitude vortices, namely two positive and two negative vortices $\kappa_1 = \kappa_2 = 1$ and $\kappa_3 = \kappa_4 = -1$. The results are summarised in figure 8 in the same format used in the previous cases. Here, up to 7 configurations may exist simultaneously (see below), so it is of comparable complexity to the equal vortex case examined first. At $I = 0$, there is one configuration only, with vortices of alternating sign equally spaced along a great circle (this is stable). For small I, this bifurcates into a stable configuration **2-2**$^-$**ss** with two positive vortices in the $y = 0$ plane at $z = z_a$ and two negative vortices in the $x = 0$ plane at $z = -z_a$ (here $z_a = I/4$); a stable configuration **1-1**$^-$**sc** lying on a great circle ($y = 0$) with $\boldsymbol{x}_1 = (r_b, 0, -z_b)$, $\boldsymbol{x}_2 = (-r_a, 0, z_a)$, $\boldsymbol{x}_3 = (-r_a, 0, -z_a)$ and $\boldsymbol{x}_4 = (r_b, 0, z_b)$ (here $r_{a,b} = \sqrt{1 - z_{a,b}^2}$ and $z_b > z_a$); and a further *pair* of unstable configurations **1**$^-$**-2-1**$^-$ / **1-2**$^-$**-1** with two negative/positive

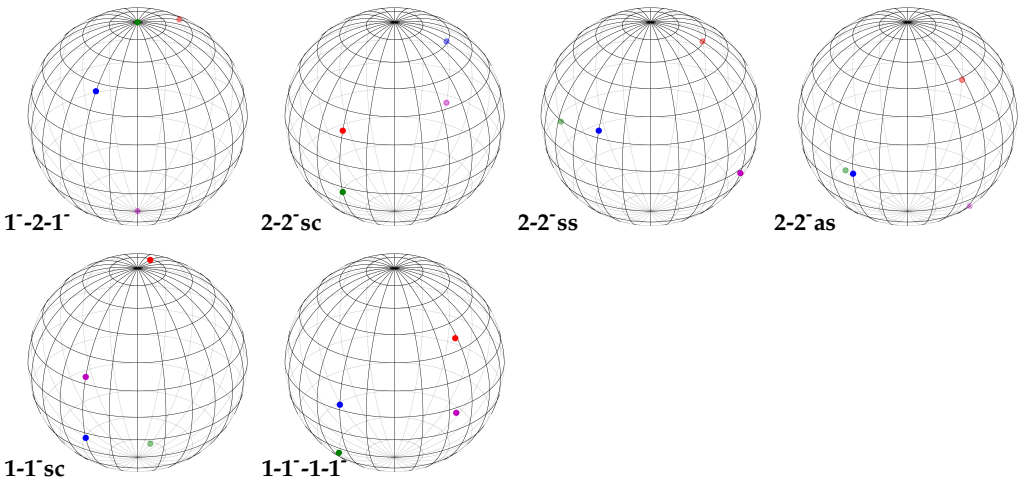

Figure 9. Illustration for $\kappa_1 = \kappa_2 = 1$ and $\kappa_3 = \kappa_4 = -1$ of the various configurations (as labelled in the lower right) that exist when $I = 1.3$. The layout is exactly as in figure 3. Vortex 1 is shown in blue, 2 in red, 3 in green and 4 in magenta.

polar vortices and two positive/negative vortices at $z = \pm I/2$. This pair of configurations has identical properties (Ω, E, etc...) so only one configuration is found by the numerical algorithm for any value of I. Notably, these configurations also counter-rotate ($\Omega < 0$ despite $I > 0$). The configuration **1-1¯sc** also counter-rotates for $I < 2$, but co-rotates for $I > 2$ (Ω diverges as $I \to 2$ in either direction). The notation "**sc**" means "symmetric in z and on a great circle", while "**ss**" means "symmetric in z but staggered (pairs of vortices lying in perpendicular planes)".

Additionally, three other unstable configurations bifurcate from the equator or the poles; all of these configurations have $\Omega \to \infty$ as $I \to 0$. The first, **2-2¯sc** consists of two vortex pairs (dipoles) straddling the equator and chasing one another; this lies on a great circle ($y = 0$) with the positive/negative vortices having $z = \pm I/4$ and opposite x. The growth rate σ_r remains close to 1 for all values of I except near $I = 3.145$ beyond which there is stability (the maximum $\sigma_r \approx 1.118034$ near $I = 2.310$). The second configuration **2-2¯as** emerges from the south pole with the two positive vortices located at $z = z_b$ in the $y = 0$ plane and the two negative vortices located at $z = z_a$ in the $x = 0$ plane, with $z_b > z_a$. This is asymmetric in z and staggered, hence the "**as**" notation. This is the most unstable configuration until about $I = 1.3$. Curiously, $\Omega = 2/I$ up to $I = 4(\sqrt{2} - 1) \approx 1.657$, where $\sigma_r \to 0$ and the configuration merges into **2-2¯ss**. This fact allows one to determine z_a and z_b from

$$z_b = \tfrac{1}{2}\alpha + \sqrt{1 - \sqrt{2}\alpha + \tfrac{1}{4}\alpha^2}\,, \qquad z_a = z_b - \alpha \quad \text{where} \quad \alpha = \tfrac{1}{2}I\,.$$

No real roots exist for $\alpha > 2(\sqrt{2} - 1)$.

The final configuration **1-1¯-1-1¯** also emerges from the south pole but has four different z positions $z_1 = -z_4 = z_b > 0$ and $z_2 = -z_3 = z_a$ with $z_b > z_a$. The configuration may be rotated about the z axis so that $y_1 = y_3 = y_b$ and $y_2 = y_4 = -y_b$, i.e. the vortex pairs $(1, 3)$ and $(2, 4)$ lie in opposite parallel vertical planes. This is the second most unstable configuration before briefly becoming the most unstable between roughly $I = 1.3$ and $I = 1.5$; it exists until $I = 2.906$ approximately, where it also merges into the unstable **2-2¯ss** configuration (with growth rate $\sigma_r \approx 1.4551$). Figure 9 provides a three-dimensional view of these configurations at $I = 1.3$.

Further properties of the **1-1¯-1-1¯** configuration are shown in figure 10. The z positions versus I form two slanted ellipses, while the angular differences $\varphi_1 - \varphi_k$ for $k > 1$ vary between 0 and π. Note, this configuration could not be found in the two gaps $0.74 \le I \le 0.88$ and $1.02 \le I \le 1.16$, which is why there is a drop in the number of states there in figure 8. Attempts failed to fill

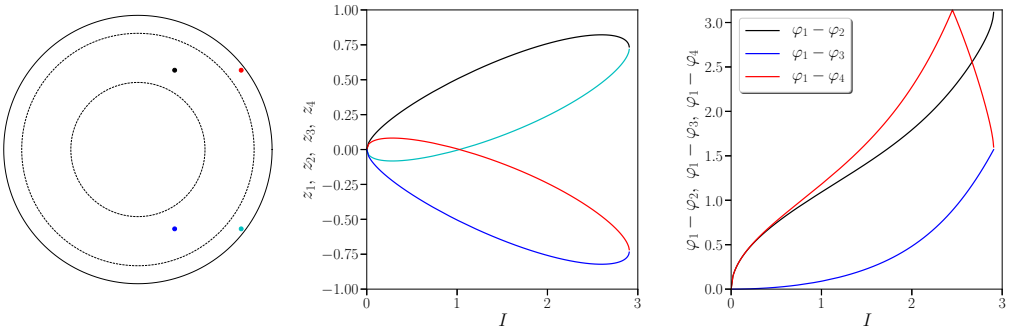

Figure 10. Projected (x, y) positions (left) of the vortices (when $\kappa_1 = \kappa_2 = 1$ and $\kappa_3 = \kappa_4 = -1$) for the **1-1¯-1-1¯** configuration at $I = 2$, with vortex 1 in black, vortex 2 in cyan, vortex 3 in red and vortex 4 in blue (with the positive vortices arranged so that $z_1 > z_2$ and the negative ones arranged so that $z_3 > z_4$); z positions of the vortices (middle) versus I; and the longitudinal angle differences between vortex 1 and the remaining vortices (right). This exists over the range $0 < I < 2.906$ approximately, and at the maximum $I = I_{\max}$ the z positions tend to $\pm I_{\max}/4$ whereas the angle differences tend to π or $\pi/2$.

these gaps using a known solution and a very small increment in I, with extrapolation between successive solutions to provide a good guess. There is no evidence of a nearby bifurcation in the diagnostics, so it is unclear why these gaps exist.

The stable **1-1¯sc** great circle configuration is the lower blue curve in $\overline{\min d_{ij}^2}$ before it merges into the stable branch of the **2-2¯sc** for $I > 3.145$ approximately. The latter is also a great circle configuration. It shares the largest $\overline{\min d_{ij}^2}$ with **2-2¯ss** (both configurations have the same z positions, but the second is staggered). For $I < 2\sqrt{2}$, $\overline{\min d_{ij}^2}$ suddenly decreases for **2-2¯sc** but continues increasing for **2-2¯ss** until reaching a peak of $8/3$ at $I = 4/\sqrt{3}$ when the vortices lie at the vertices of a regular tetrahedron. The latter configuration has the largest $\overline{\min d_{ij}^2}$ for $I < 2\sqrt{2}$, and is unstable for all $I > 4(\sqrt{2} - 1) \approx 1.657$ (this is the example featured in figure 1(a)). It also has the smallest positive Ω for all I, and in $\min \overline{d_\circ^2}$ is seen as the upward sloping blue curve until $I = 1.657$ and the uppermost red curve thereafter. The maximum $\sigma_r \approx 1.4860185$ and is attained near $I = 3.287$.

The pair of unstable configurations **1¯-2-1¯** / **1-2¯-1** having two negative/positive polar vortices is seen as the downward sloping straight red line in $\min \overline{d_\circ^2}$ up to $I = 2$, where the configurations cease to exist (and $\sigma_r \to \infty$). These are great circle configurations so $\min \overline{d_\circ^2} = 0$. For $I > 2$, a new configuration **1-1-2¯** emerges from three vortices at the south pole and a positive vortex at the north pole (E, Ω and σ_r all diverge as $I \to 2$). The positive vortices are in the $y = 0$ plane at positions $(-\sqrt{1 - z_1^2}, 0, z_1)$ and $(\sqrt{1 - z_2^2}, 0, z_2)$ with $z_2 < z_1$. The negative vortices are at the same height $z_3 < z_2$ at positions (x_3, y_3, z_3) and $(x_3, -y_3, z_3)$, with $x_3 > 0$ in general. This configuration is unstable until it merges into **2-2¯ss** around $I = 2.906$, along with **1-1¯-1-1¯**. That is, the two most asymmetric configurations merge into the symmetric-staggered one at this value of I. Beyond $I = 3.145$ approximately, only the **2-2¯ss** and **2-2¯sc** configurations remain, and only the latter is stable.

(iv) Slightly unequal vortices: $\kappa_2/\kappa_1 = \kappa_3/\kappa_2 = \kappa_4/\kappa_3 = 0.9$

We next consider a more complex case when all of the vortex strengths are comparable but slightly different ($\kappa_{i+1}/\kappa_i = 0.9, i = 1,\ 2,\ 3$). In this case, all symmetry is broken and many more equilibria exist for a given I than for exactly equal vortices.

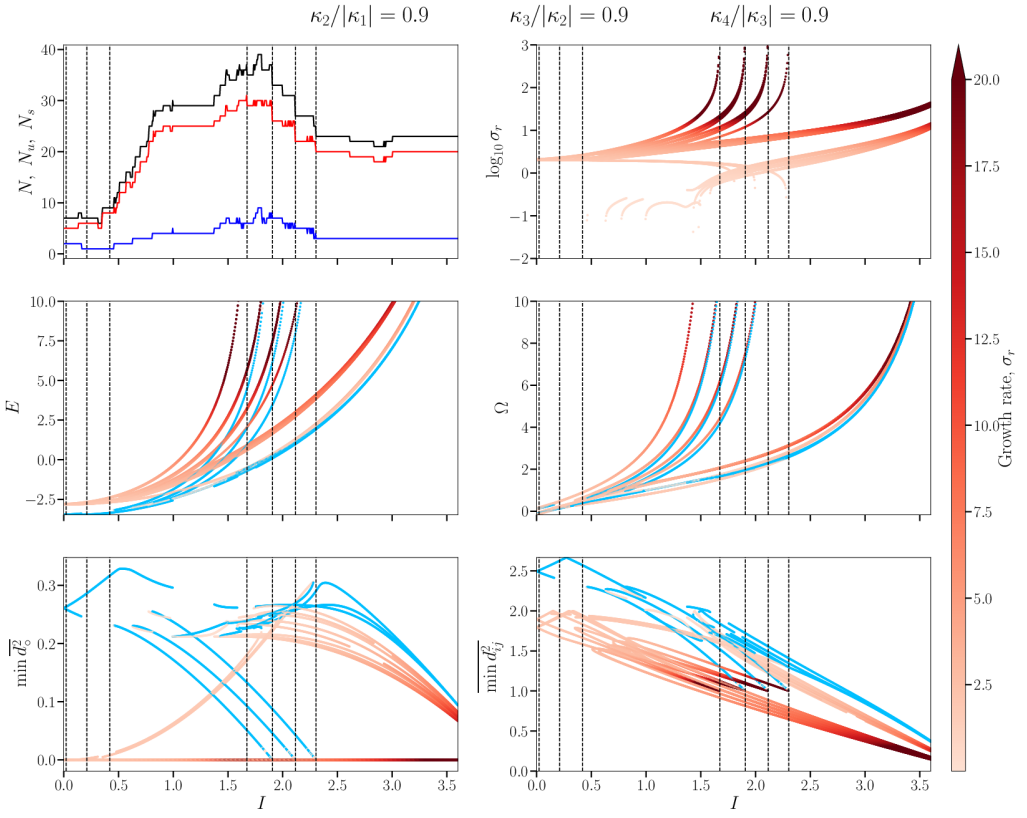

Figure 11. Various properties of point vortex equilibria, as a function of the z component of angular impulse I, for $n = 4$ vortices and for strength ratios $\kappa_{i+1}/\kappa_i = 0.9$, $i = 1,\ 2,\ 3$ (the sum of the strengths is always $n = 4$). The layout of the figure is exactly as described in figure 2.

This is shown in figure 11. This is in fact not the most complex case found — up to 47 equilibria occur when all the strength ratios are 0.999 (compared to 46 equilibria for $\kappa_{i+1}/\kappa_i = 0.99$). However, the present case allows one to see more clearly the individual equilibria. Comparing with the equal-vortex case in figure 2, one can see many similarities in the diagnostic quantities. Each curve in figure 2 opens up into many curves in figure 11. Up to 12 different equilibria can bifurcate from a single equilibrium in the equal-vortex case (and perhaps more — it is difficult to check this for all equilibria). For example, the single (unstable) **2-2c** configuration for equal vortices where the vortices lie on a great circle, and with pairs of vortices having equal z, bifurcates into 12 different (unstable) great circle configurations at $I = 3.6$. The vertical lines in figure 11 are the critical values of I (see (4.6)) where two or more vortices are at either pole. At these values, both the energy E and rotation rate Ω diverge, and the growth rate σ_r either diverges or goes to zero. For small I, some of the equilibria counter-rotate ($\Omega < 0$), unlike in the case of equal vortices. Examination of the case having strength ratios of 0.99 indicates that there are no new equilibria which are unrelated to those occurring for equal vortices.

(v) Mixed vortices I: $\kappa_2/|\kappa_1| = -1$, $\kappa_3/|\kappa_2| = -0.8$ and $\kappa_4/|\kappa_3| = 0.75$

We next consider a case previously studied in [15], examining integrable point vortex motion for $n = 4$. Integrability requires $I = 0$, which is a special case in the full parameter space studied here. The specific case considered is the one with circulations $\Gamma_1 = 5$, $\Gamma_2 = 3$, $\Gamma_3 = -4$ and $\Gamma_4 = -5$ in [15], which was found to induce 'topological chaos' by exhibiting a 'pseudo-Anosov' braid in

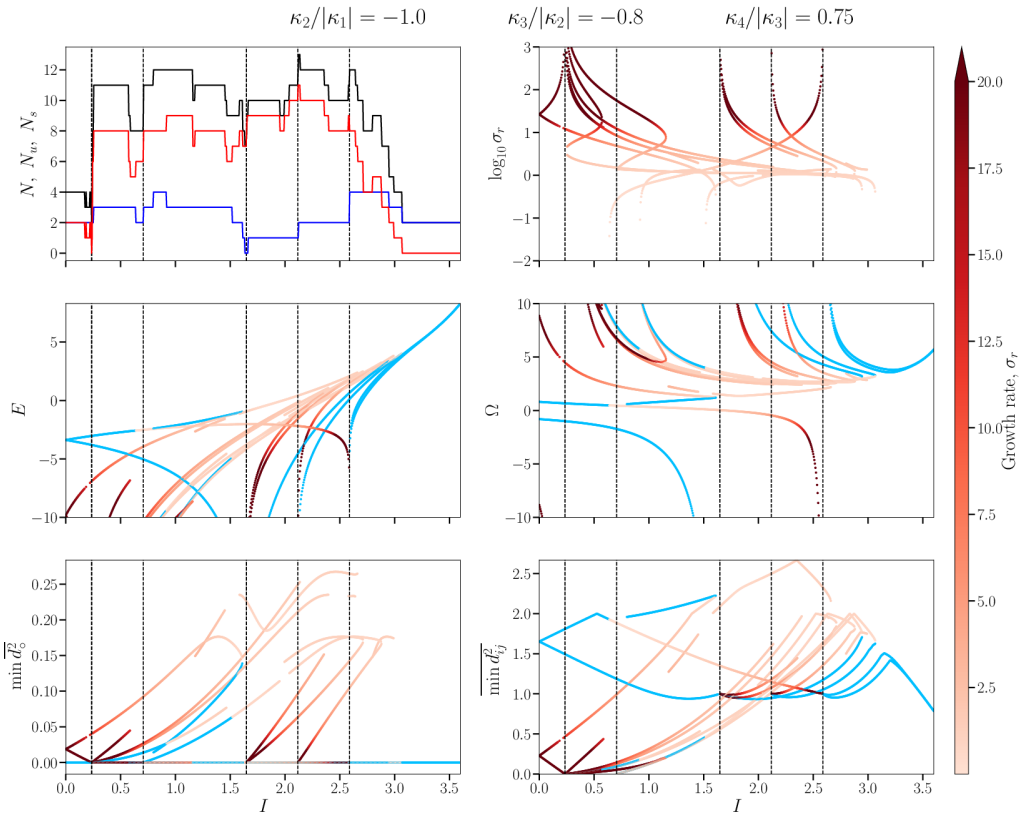

Figure 12. Various properties of point vortex equilibria, as a function of the z component of angular impulse I, for $n = 4$ vortices and for strength ratios $\kappa_2/|\kappa_1| = -1$, $\kappa_3/|\kappa_2| = -4/5$, and $\kappa_4/|\kappa_3| = 3/4$. The layout of the figure is exactly as described in figure 2.

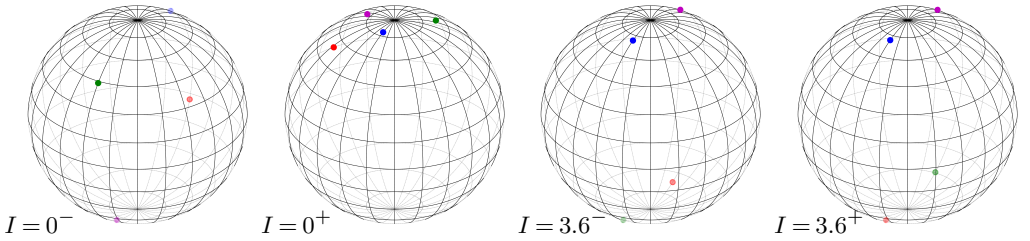

Figure 13. Illustration for $\kappa_2/|\kappa_1| = -1$, $\kappa_3/|\kappa_2| = -4/5$, and $\kappa_4/|\kappa_3| = 3/4$ of the various configurations that exists at both ends of the range in I (as labelled in the lower right). A $-/+$ superscript indicates the state with lower/higher Ω. The layout is exactly as in figure 3. Vortex 1 is shown in blue, 2 in red, 3 in green and 4 in magenta.

its dynamical evolution. The point vortices themselves do not move chaotically in this case, but passive particles between them may.

In our notation, this case has $\kappa_2/|\kappa_1| = -1$, $\kappa_3/|\kappa_2| = -4/5$ and $\kappa_4/|\kappa_3| = 3/4$, and its equilibrium properties (for $0 \leq I \leq 3.6$) are displayed in figure 12. This case exhibits at most 13 distinct equilibria and is exceptional in that only stable equilibria exist for large I (many other examples have been considered, including four other from [15,16]).

When $I = 0$, the integrable case, two pairs of identical equilibria exist. One of them is the equatorial ring considered by [15], however in our arrangement this is rotated in the $y = 0$ plane. This is shown in the left panel of figure 13. This configuration is linearly stable and rotates at the angular frequency $\Omega = 0.8098936139$. By symmetry, there exists another identical configuration with all $\boldsymbol{x}_i \to -\boldsymbol{x}_i$ and $\Omega \to -\Omega$. There is also an unstable pair of equilibria, one near the north pole with $\Omega = 8.8402886518$ (see second to left panel in figure 13), and another identical configuration with all $\boldsymbol{x}_i \to -\boldsymbol{x}_i$ and $\Omega \to -\Omega$. These have large growth rates, $\sigma_r = 26.6468$. For small I, these pairs of equilibria split into distinct equilibria with no symmetry. The stable one with $\Omega < 0$ remains stable and in a great-circle configuration ($y = 0$) until it ceases to exist around $I = 1.64706$ when the opposite pair of vortices 1 and 2 merge (annihilate) at $\boldsymbol{x} = (1, 0, 0)$ while the negative vortex 3 moves to the south pole and the positive vortex 4 moves to the north pole. The other stable one with $\Omega > 0$ at $I = 0$ is also a great-circle configuration, but becomes unstable around $I = 0.638$ and progressively more unstable until it ceases to exist around $I = 2.58824$ when vortex 1 reaches the north pole and the remaining three vortices reach the south pole ($E,\ \Omega \to \infty$ and $\sigma_r \to \infty$).

At the other extreme, when $I = 3.6$, only two stable configurations exist. These closely resemble each other except that the x coordinates of vortices 2 and 3 are nearly opposite one another — see right two panels in of figure 13. As $I \to 4$, it is expected that vortices 1 and 4 reach the north pole, while vortices 2 and 3 reach the south pole.

(vi) Mixed vortices II: $\kappa_1 = 1.6$, $\kappa_2 = 1.2$, $\kappa_3 = -0.8$ and $\kappa_4 = -0.4$

The final case discussed has two stronger positive vortices ($\kappa_1 = 1.6$, $\kappa_2 = 1.2$) and two weaker negative vortices ($\kappa_3 = -0.8$, $\kappa_4 = -0.4$). This case displays an unusual pattern of equilibria compared with many other cases examined.

The results are shown in figure 14. Here the critical values of I (the vertical dashed lines) are equally spaced at intervals of 0.8. This case is distinctive in having an abrupt jump in the number of equilibria at $I = 1.6$, where 7 new (unstable) equilibria arise. There are also many counter-rotating configurations, and one at surprisingly large I, in the range $1.29 < I < 1.6$, seen as the looping structure in many of the diagnostics. This configuration is highly unstable, with growth rates σ_r around 40 or greater. This emerges just before $I = 1.29$ with the strongest positive vortex at the north pole, and the remaining vortices all in the northern hemisphere (in fact the minimum z is 0.332, and this corresponds to the second strongest positive vortex). There is no evident symmetry.

For small I, including $I = 0$, there are two stable and two unstable configurations. The stable configurations lie on a great circle ($y = 0$) with the two positive vortices in opposite hemispheres near (but not at) the two poles, and the negative vortices in the same hemisphere occupied by the positive vortex which is closer to the equator. When $I = 0$, the configurations are mirror images of each other through $z = 0$, and have opposite Ω. The two unstable configurations ($\sigma_r = 5.95$ approximately) have no evident symmetry. The strongest vortex is in one hemisphere and the remaining vortices are in the other. Again, the two configurations are mirror images of each other when $I = 0$ and have opposite Ω.

For large I, specifically $I > 3.2$, there are just three configurations, two of which are stable. They all have similar properties apart from σ_r and $\min \overline{d_\circ^2}$. They converge to a configuration in which the positive vortices are at the north pole and the negative vortices are at the south pole as $I \to 4$. The stable configurations lie on a great circle ($y = 0$), while the unstable configuration has no evident symmetry (and $\min \overline{d_\circ^2} > 0$).

This case is also interesting in that over $1.16 \leq I \leq 1.285$ only one equilibrium was found (except for a small interval). This could be numerical: there is no guarantee that all equilibria can be found by the algorithm developed. Also, over an extensive range of I, from approximately $I = 0.975$ to 2.4, no stable equilibria appear to exist (again except for a small interval). Here, as in many other cases examined for general circulation ratios, the number of unstable equilibria is often many times greater than the number of stable equilibria, apart from near the endpoints in I.

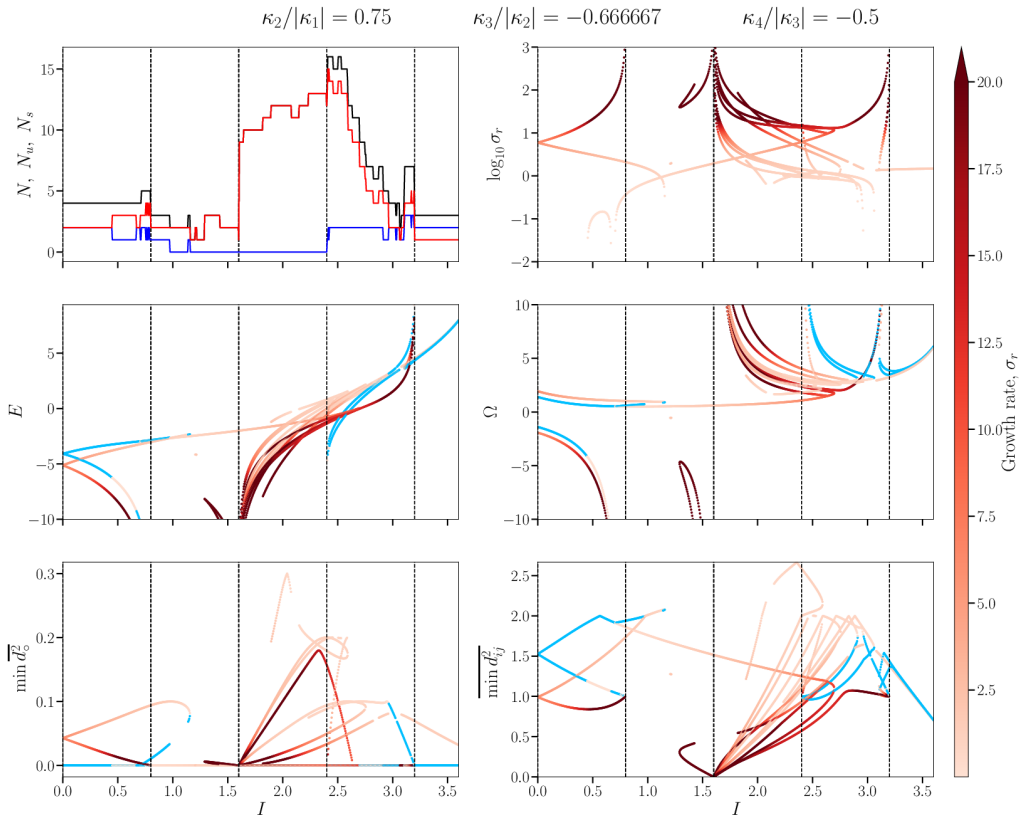

Figure 14. Various properties of point vortex equilibria, as a function of the z component of angular impulse I, for $n = 4$ vortices and for strength ratios $\kappa_2/|\kappa_1| = 3/4$, $\kappa_3/|\kappa_2| = -2/3$, and $\kappa_4/|\kappa_3| = -1/2$. The layout of the figure is exactly as described in figure 2.

5. Nonlinear dynamics

With the myriad of unstable equilibria, it is impossible to comprehensively study the nonlinear evolution of the instabilities. We would especially like to know how generic chaotic motion is, and if such motion is characteristic of inviscid flow on a sphere, as suggested by [7]. There, it was found that the late-time behaviour of inviscid two-dimensional turbulence on a sphere remains unsteady, and it was demonstrated that the underlying mechanism is closely linked with point vortex dynamics. Mathematically, chaotic motion has been demonstrated for 6 or more vortices in [18], but 4 and 5 vortices appear to be more difficult to analyse. Below, we provide numerical evidence that the 4 vortex problem is generally non-integrable and that the vortex motion is generally chaotic. Any comprehensive analysis of the potential forms of motion is out of the question, as the problem depends on the three strength ratios, the angular impulse, and the specific equilibrium state studied (and there may be tens of these for a given set of parameters). Instead, a few examples will be provided to give a glimpse of the diverse forms of evolution.

First of all, the equations of motion (2.2), in a frame of reference rotating with the equilibrium rotation rate, are time integrated using the 4th-order Runge-Kutta method, with time step adaption. First, we require $\Omega_{\max}\Delta t < 0.02$ where Δt is the time step and

$$\Omega_{\max} = \max_{i \neq j} \left(\frac{\|(\boldsymbol{x}_i - \boldsymbol{x}_j) \times (\boldsymbol{u}_i - \boldsymbol{u}_j)\|}{\|\boldsymbol{x}_i - \boldsymbol{x}_j)\|^2} \right) \tag{5.1}$$

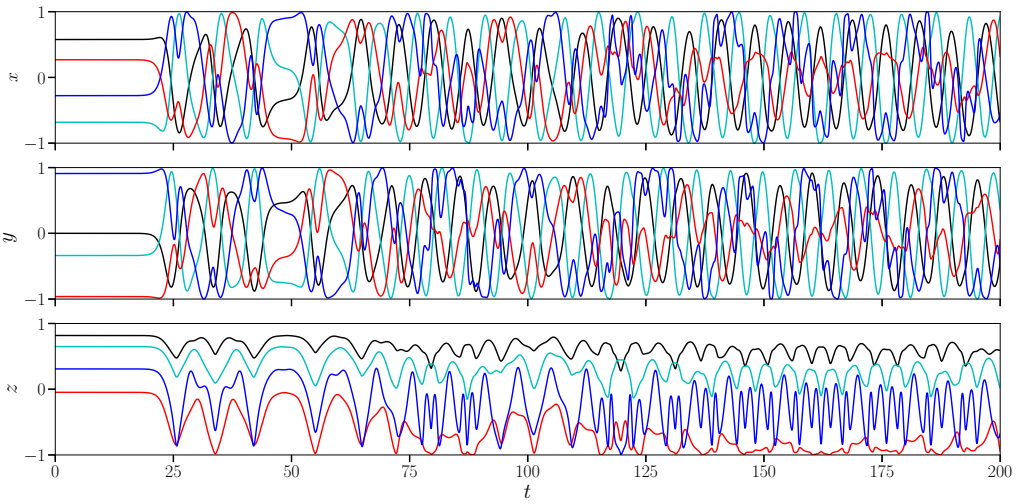

Figure 15. Evolution of the x, y and z coordinates (top to bottom) of four point vortices with $\kappa_1 = 1.6$, $\kappa_2 = 1.2$, $\kappa_3 = -0.8$ and $\kappa_4 = -0.4$, starting from the least unstable (near-) equilibrium configuration when $I = 2.0$. Vortex 1 is shown in black, 2 in cyan, 3 in red and 4 in blue.

is the maximum rotation rate of any pair of vortices (i, j). Second, we require $U_{\max}\Delta t < 0.005$ where

$$U_{\max} = \max_j \|\boldsymbol{u}_j\| \tag{5.2}$$

is the maximum speed of any vortex. These requirements generally lead to energy variations of less than 10^{-8} and angular impulse variations of less than 10^{-10}.

The first example illustrated is for the mixed vortex case $\kappa_1 = 1.6$, $\kappa_2 = 1.2$, $\kappa_3 = -0.8$ and $\kappa_4 = -0.4$ discussed at the end of the previous section. We consider $I = 2$ where no configuration is stable, but focus on the least unstable of the 12 configurations found. This one has $\sigma_r = 1.163$ approximately. The evolution of the vortices is difficult to visualise on the full sphere as in figure 1(b) due to the complexity of the trajectories. Instead, we show the individual coordinates of the vortices as a function of time t in figure 15. The instability grows entirely from numerical noise, so the vortices remain nearly stationary (in the co-rotating frame) until around $t = 20$. Thereafter, the vortices move in an increasingly irregular manner, with the strongest negative vortex (in red) moving close to the south pole at late times, and the weaker negative vortex (in blue) exhibiting large excursions in z. This is not proof that the evolution is chaotic, but the potential for chaos exists, and from a wide exploration many unstable equilibria evolve in a similarly irregular manner. A power spectrum of the z coordinates of the vortices in figure 16 shows a broad range of excited frequencies, which would unlikely occur in quasi-periodic motion.

The second example illustrated is for the case $\kappa_1 = \kappa_2 = \kappa_3 = 1$ and $\kappa_4 = -1$, also studied in the previous section (see e.g. figure 5). We consider the unstable configuration shown in the left panel of figure 7 for $I = 2.5$. This has a growth rate of $\sigma_r = 0.8006$ approximately.

The time evolution of the vortex coordinates until $t = 200$ is shown in figure 17. As the instability grows from numerical noise, it takes longer for it to manifest itself compared to the previous example which had a growth rate nearly 50% larger. Just after $t = 30$, the two initially equal-height positive vortices (in black and cyan) separate. Thereafter the remaining positive vortex (in red) oscillates in the same height range as the more northerly vortex (in cyan). The negative vortex (in blue) remains near the south pole. While some regularity may be seen in the oscillations, a much longer integration to $t = 10000$ in fact produces a power spectrum closely similar to that seen in the previous case in figure 16. The spectrum is relatively flat for

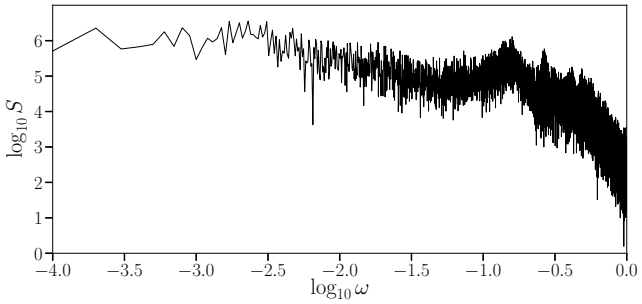

Figure 16. Average frequency power spectrum $S(\omega)$ of $z_j(t)$ (averaged over j) for the evolution shown at early times in figure 15. Here, the integration range has been extended to $t = 10000$ to better resolve low frequencies ω. At higher frequencies than shown, the spectrum $S(\omega)$ continues to decay rapidly with ω, roughly as ω^{-6}.

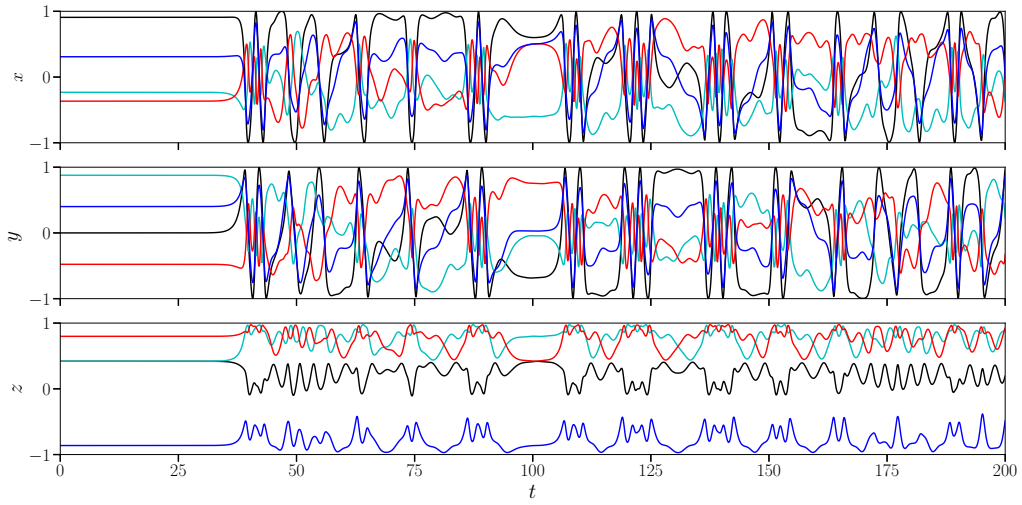

Figure 17. Evolution of the x, y and z coordinates (top to bottom) of four point vortices with $\kappa_1 = \kappa_2 = \kappa_3 = 1$ and $\kappa_4 = -1$, starting from the unstable (near-) equilibrium **2-1˙-1** configuration when $I = 2.5$ (this corresponds to the unfilled circles in the left panel of figure 7). Vortex 1 is shown in black, 2 in cyan, 3 in red and 4 in blue.

$\log_{10} \omega < -0.5$, or $\omega < 0.3$ approximately, indicating that there is a very wide range of active frequencies exhibited by the evolution, suggesting chaotic dynamics.

The final example considers two pairs of opposite vortices, $\kappa_1 = \kappa_2 = 1$ and $\kappa_3 = \kappa_4 = -1$, in the **1-1˙-1-1˙** configuration studied in figure 10. Specifically, we consider $I = 2$ shown in the left hand panel of that figure. This has a growth rate of $\sigma_r = 1.4608$ approximately. The evolution of the vortex coordinates is shown in figure 18. The instability becomes evident by $t = 20$, and thereafter the evolution is erratic, passing through phases of relative order like $50 < t < 60$ when the z coordinates of the like-signed vortices remain nearly equal, then on to much more dynamic phases like $72 < t < 75$ when three of the four vortices exhibit rapid and large excursions in z. As in the previous cases, the power spectrum of the dynamics out to much later times is nearly flat for frequencies $\omega < 0.1$, suggesting chaotic behaviour.

An animation of the vortex motion suggests that the vortices are equally likely to be anywhere on the spherical surface. To quantify this, simulations were conducted starting from the same

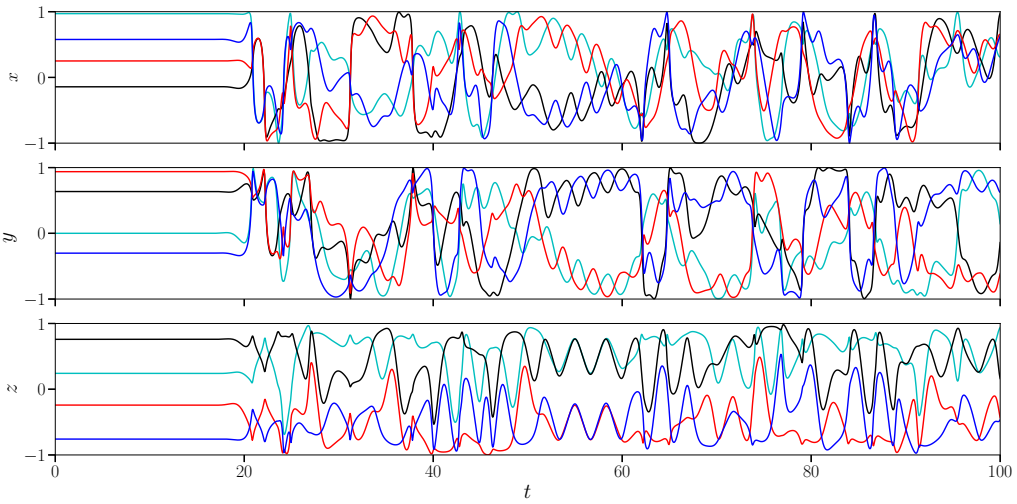

Figure 18. Evolution of the x, y and z coordinates (top to bottom) of four point vortices with $\kappa_1 = \kappa_2 = 1$ and $\kappa_3 = \kappa_4 = -1$, starting from the unstable (near-) equilibrium **1-1⁻-1-1⁻** configuration when $I = 2$ (this corresponds to the case illustrated in the left panel of figure 10). Vortex 1 is shown in black, 2 in cyan, 3 in red and 4 in blue.

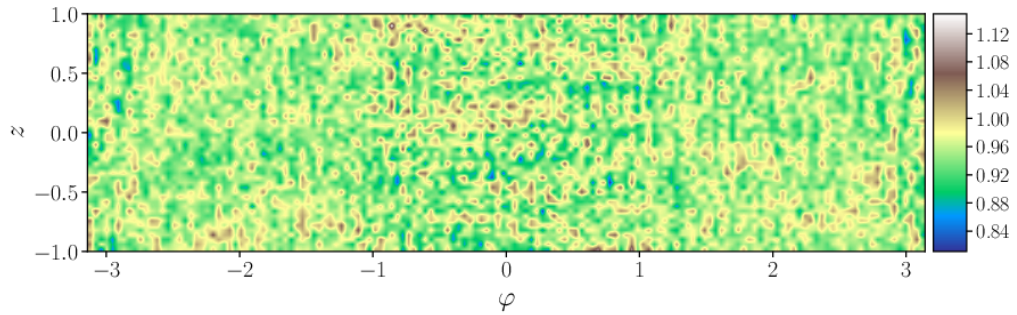

Figure 19. Probability $P(\varphi, z)$ of finding a vortex at any specific longitude φ and height z, in a simulation carried out to $t = 100000$ for the configuration examined in figure 18 at relatively early times. See text for further details.

initial conditions but taken to different ending times, $t = 1000$, 10000 and 100000. The time step was reduced to 0.3 of its standard setting to ensure accuracy over these long integration times (energy is conserved to within 5×10^{-8} (the initial energy $E = -0.889632181$), while the angular impulse vector is conserved to within 8×10^{-9}). At the end of each time step, the vortex positions were binned into equal-area rectangles $\Delta\varphi\,\Delta z$ (bins) in longitude φ and height z. Specifically, each time a vortex was found in a specific bin, the time step Δt was added to that bin to give a measure of how long the vortex spent in that bin. The results were then normalised to give the probability $P(\varphi, z)$ of finding a vortex at a specific longitude φ and height z (here 150 bins are used in φ and 50 in z).

The results for the longest integration time to $t = 100000$ are presented in figure 19 (note: the vortex positions were binned only for times $t > 20$ when the instability has reached a mature stage, see figure 18). The probability $P(\varphi, z)$ is everywhere close to 1, with a variance of 0.038, confirming the visual impression that the vortices visit all parts of the sphere with equal

probability. At shorter integration times, similar results are found but the variances are 0.121 and 0.369 for $t = 10000$ and $t = 1000$ respectively. The variances diminish like $1/\sqrt{t}$, just as would be found by randomly placing a point $\propto t$ times. This strongly suggests that $P \to 1$ as $t \to \infty$. Moreover, the power spectrum (not shown) exhibits a nearly flat spectrum extending to the lowest frequencies considered ($\omega = 10^{-5}$). Again, this is evidence for chaotic motion.

The erratic motion exhibited by the three examples considered is not rare — almost every example of the hundreds investigated exhibits aperiodic, potentially chaotic dynamics. The few exceptions occur for highly symmetric cases, like for all equal vortices lying on a ring of constant latitude, which evolves nearly periodically, with opposite vortices staying at the same heights (while varying in time) and 180° apart in longitude. This is exceptional however. Without symmetry, it is plausible that chaotic dynamics is the norm, but the parameter space is too vast to verify this.

6. Discussion

This paper has presented a general approach to calculating the linear stability of an arbitrary (relative) equilibrium of point vortices on the surface of a sphere. The approach works for any number of vortices having arbitrary circulations. This approach was then adapted to determine equilibria. The fundamental idea is to make a starting guess consistent with the chosen angular impulse I (in the positive z direction), and with one vortex held at a longitude of 0 (to avoid duplicate equilibria), then iterate this guess by displacing the vortices towards equilibrium. This may not work for a particular starting guess (the iteration diverges), in which case another is tried. Eventually, the method succeeds in finding an equilibrium. However, it is rejected if it is the same as any other previously found for the chosen angular impulse.

This approach to finding equilibria is distinct from the "Brownian ratchet" one developed by [12] and [13] for the same purposes. The advantage of the new approach presented here is that all (or nearly all) equilibria can be found for a specific angular impulse I, and I can be varied over its full range to follow the bifurcation structure occurring for a specific set of vortex strengths (circulations divided by 4π). The sum of the vortex strength magnitudes is taken to be n without loss of generality; then $0 \le I \le n$ is sufficient to describe all possible equilibria.

For $n = 4$ vortices, the focus of this study, the minimum number of equilibria found was 1 while the maximum number found was 47, across all I and across a wide range of cases having different vortex circulation ratios. The minimum occurs not only for certain symmetric cases like all equal vortex strengths at the special value $I = 0$, but also for mixed-strength cases at intermediate I. The maximum of 47 was found for nearly equal vortices with strength ratios of 0.999 (this is likely to persist for strength ratios even closer to 1). Notably, for equal strength vortices, the maximum number of equilibria is just 7. These solutions bifurcate into many additional solutions for strength ratios < 1 (up to 12 have been observed to bifurcate from a single equilibrium). Most of these solutions are linearly unstable however.

Interestingly, for $n = 3$ vortices, the maximum number of equilibria found is just 7, again for vortices with strength ratios just less than 1 (no results have been included here). For equal vortices, the maximum number of equilibria is just 3. A thorough examination of the three-vortex problem can be found in [2,10,11].

The focus on 4 vortices here was motivated by an earlier study investigating the late time behaviour of two-dimensional turbulence on a sphere [7], where four dominant unsteady vortices were seen to emerge and persist. This unsteady behaviour was accurately reproduced by 4 point vortices of specific circulations, indicating that the point vortex problem is an appropriate reduced model for the flow at late times. Nonlinear simulations of a large number of unstable point vortex configurations conducted for the present study indicate that unsteadiness is generic, and moreover, the motion is likely to be chaotic. Two examples were shown, but the counter-examples are rare, occurring only for highly symmetric configurations like latitudinal rings of equal vortices. The implication is that inviscid two-dimensional turbulence on a sphere likely

evolves, generically, into a chaotic large-scale flow characterised by the erratic motion of four dominant vortices.

A challenging problem for future work is to determine the maximum number of equilibria possible for n vortices, for arbitrary vortex strengths and angular momentum. Here, numerical evidence alone indicates that this maximum is 7 for $n=3$ and 47 for $n=4$. Limited investigation has been carried out for $n=5$, but a maximum of 207 is found when all circulation ratios are 0.999, the case which produces the most equilibria for $n=4$ and 3. Suffice it to say, investigating $n>4$ is much more complicated! On the other hand, the computational cost does not appear to depend strongly on n. For example, when all of the strength ratios $\kappa_{j+1}/\kappa_j = 0.9$, the algorithm developed takes 6.64, 35.5, 44.3, 25.3 and 22.9 hours, respectively for $n=3$, 4, 5, 6 and 7 vortices. Meanwhile, respectively 2435, 17099, 130895, 213299 and 253606 equilibria were obtained. This translates into 9.81, 7.48, 1.21, 0.427 and 0.324 seconds required per equilibrium. The cost is non-monotonic in n (at least for this choice of vortex strengths), but indicates that the algorithm may be more efficient as n increases. It therefore appears to offer a viable new approach for studying larger n.

Another challenging problem is finding vortex equilibria on general surfaces of revolution, such as closed surfaces [8], multiply-connected surfaces like the torus [17], or open surfaces like the cone and paraboloid [9]. For surfaces of revolution, the conformal map required for deriving the equations of motion is known explicitly, making their linearisation straightforward in principle and opening the way for applying the present approach to finding equilibria. Two significant modifications are required however. The first comes from the fact that only the axial component of the angular impulse is conserved (there is only one rotational symmetry on a general surface of revolution). Hence, there are two fewer constraints to satisfy. This simply means that two of the rows in the linearised problem are *not* replaced as in (3.5). Moreover, the axial component of angular impulse is no longer $\sum_i \kappa_i z_i$ but rather $\sum_i \kappa_i \mu_i$ where μ is the appropriate coordinate for which $\mathrm{d}\mu\,\mathrm{d}\varphi$ expresses differential area. The second modification is to randomly choose μ_i rather than z_i from a uniform distribution when generating a starting guess. The extension of the present algorithm in this way may offer an efficient approach to finding many new vortex equilibria, especially configurations having no symmetry.

Ethics. There are no ethical considerations.

Data Accessibility. Please contact the author for the numerical codes used.

Competing Interests. The author declares that he has no competing interests.

Funding. Support for this research has come from the UK Engineering and Physical Sciences Research Council (grant EP/H001794/1).

Acknowledgements. The suggestions of two anonymous referees are gratefully appreciated.

References

1. Aref H, Vainchtein D 1998. Point vortices exhibit asymmetric equilibria. *Nature* **392**, 769–770.
2. Borisov AV, Mamaev IS, Kilin AA 2018. Dynamics of three vortices on a sphere. *Regul. Chaot. Dyn.* **23**, 127–134.
3. Boatto S, Simó C 2004. Stability of latitudinal vortex rings with polar vortices. Preprint, pp. 1-44. See http://www.ma.utexas.edu/mp_arc/a/04-67.
4. Boatto S, Simó C 2019. A vortex ring on a sphere: the case of total vorticity equal to zero. *Phil. Trans. R. Soc. A* **377**, 20190019.
5. Campbell LJ, Ziff RM 1979. Vortex patterns and energies in a rotating superfluid. *Phys. Rev. B* **20(5)**, 1886–1902
6. Dritschel DG 1985. The stability and energetics of corotating uniform vortices. *J. Fluid Mech.* **157**, 95–134.
7. Dritschel DG, Qi W, Marston, JB 2015. On the late-time behaviour of a bounded, inviscid two-dimensional flow. *J. Fluid Mech.* **783**, 1–22.
8. Dritschel DG, Boatto S 2015. The motion of point vortices on closed surfaces. *Proc. R. Soc. A* **471**, 20140890.

9. Dritschel DG, Boatto S 2015. Point vortex dynamics on open surfaces of revolution mappable to the plane. *Proc. R. Soc. A* (submitted).
10. Kidambi R, Newton PK 1998. Motion of three point vortices on a sphere. *Physica D: Nonlinear Phenomena* **116(1)**, 143–175.
11. Newton PK 2001. The N-vortex Problem: Analytical Techniques. *Applied Math. Sci.* **45**, Springer-Verlag, New York.
12. Newton PK and Sakajo T 2009. Point vortex equilibria on the sphere via Brownian ratchets. *Proc. R. Soc. A* **465**, 437–455.
13. Newton PK and Sakajo T 2011. Point vortex equilibria and optimal packings of circles on a sphere. *Proc. R. Soc. A* **467**, 1468–1490.
14. Polvani LM and Dritschel DG 1993. Wave and vortex dynamics on the surface of the sphere: Equilibria and their stability. *J. Fluid Mech.* **255**, 35–64.
15. Sakajo T 2007. Integrable four-vortex motion on sphere with zero moment of vorticity. *Phys. Fluids* **19(1)**, 017109.
16. Sakajo T 2008. Non self-similar, partial and robust collapse of four point vortices on a sphere. *Phys. Rev. E* **78(1)**, 016312.
17. Sakajo T and Shimizu Y 2016 Point vortex interactions on a toroidal surface. *Proc. R. Soc. A* **472**, 20160271.
18. Sakajo, T and Yagasaki, K 2008. Chaotic motion of the N-vortex problem on a sphere: I. Saddle-centers in two-degree-of-freedom Hamiltonians. *J. Nonlinear Sci.* **18(5)**, 485–525.